

Radiative Corrections to Elastic and Inelastic $e\bar{p}$ and $\nu\bar{p}$ Scattering*

L. W. MO, Y. S. TSAI

Stanford Linear Accelerator Center, Stanford University, Stanford, California

We have investigated and improved the reliability of many formulas used in the radiative corrections to elastic and inelastic electron scatterings when only the scattered electrons are detected. The radiative corrections to muon scattering are also investigated. A practical and reliable recipe for unfolding the entire inelastic spectra, including effects due to virtual photons, internal and external bremsstrahlungs, is given. Examples of actually unfolding the inelastic electron spectra are given using the experimental data obtained by the electron-scattering group at the Stanford Linear Accelerator Center.

I. INTRODUCTION

Electron-proton inelastic scattering experiments are expected to yield information such as

- (1) The form factors associated with the γNN^* vertices for various N^* 's.
- (2) The sum rules¹ for γ (off shell) + $P \rightarrow$ hadrons.
- (3) Test of PCAC theory near pion threshold.²

However, a casual glance at the data from various laboratories^{3,4} shows that these resonances and continuous hadronic states sit on top of very high radiative tails, especially in the deep inelastic region, as shown⁴ in Fig. 1. Obviously, no reliable information can be extracted from such experiments unless one can calculate these radiative tails accurately. For example, when the contribution of the radiative tail amounts to 60% of the cross section, one might make an error of a factor of 2 in evaluating the hadronic cross section if an error of 20% is made in estimating the radiative tail. Various people^{3,5-11} have used different approximation schemes to evaluate the radiative tail. These approximations essentially consist of various versions of peaking approximations which assume that the photons emitted are either along the direction of the incident electron or the scattered electron. It was shown by Maximon and Isabelle¹² for the case of potential scattering that the peaking approximation can be wrong by as much as a factor of 2 in the very inelastic region. The purpose of this paper is to give a *practical* and *reliable* recipe for handling the problems associated with radiative corrections. By *practical* we mean that the problem can be handled by a computer without straining its capacity; and by *reliable* we mean that the error involved in our approximations will be small and its magnitude can be estimated. In any practical application of the radiative corrections, the effect of electron straggling in the target has to be included. This is necessary because the internal bremsstrahlung has *roughly* the same effect as that given by two external radiators with one placed before and one after

the scattering, each of thickness

$$t_{i,f} = \frac{3}{4}(\alpha/\pi)[\ln(-q^2/m^2) - 1]$$

radiation lengths. For example, if $-q^2 = 2$ GeV², these two radiators will each have a thickness of $t_{i,f} = 0.0276$ radiation lengths. If the target has thickness 0.0552 radiation lengths, the effect due to straggling will be roughly equal to that due to the radiative corrections. Hence when the target thickness is comparable to $t_{i,f}$, we must treat the straggling effect with great care.

Throughout this paper we restrict ourselves to one-photon exchange between the electron current and hadron current and also ignore the emission of real photons by hadrons. Only when treating the radiative corrections to the elastic peak have we included both the infrared divergent part of the two-photon exchange diagrams and also the emission of real photons by hadrons (see Sec. II). The order of magnitude of these effects can be estimated by comparing the Z^1 and the Z^2 terms with the Z^0 terms given in Table I.

In this paper most of the basic formulas are given in the Appendices. In the text we discuss how these formulas are to be used in practical applications. Appendix A discusses the straggling of the electrons in the target; in Appendix B we reproduce the formulas, first given by one of us (Tsai) in Ref. 13, for the exact treatment of bremsstrahlung in the lowest-order Born approximation allowing for form factors, recoil, and inelastic excitation of the target system; Appendix C derives a peaking approximation formula based on the exact formulas given in Appendix B; and in Appendix D we give several practical considerations associated with programming some of our formulas for a computer. In Sec. II, we discuss the radiative corrections to the elastic peak with the straggling effect in the target included. The numerical values from the formula of Tsai¹⁴ and that of Meister and Yennie¹⁵ for the radiative corrections to the elastic peak are compared. We found that, for $e^{\pm}\bar{p}$ scattering, the two formulas give identical answers within 1% of the cross section, but for high Z targets the results can be quite different. The origins of the differences in these two formulas are investigated. We also briefly mention how to do radiative

* Work supported by the U.S. Atomic Energy Commission.

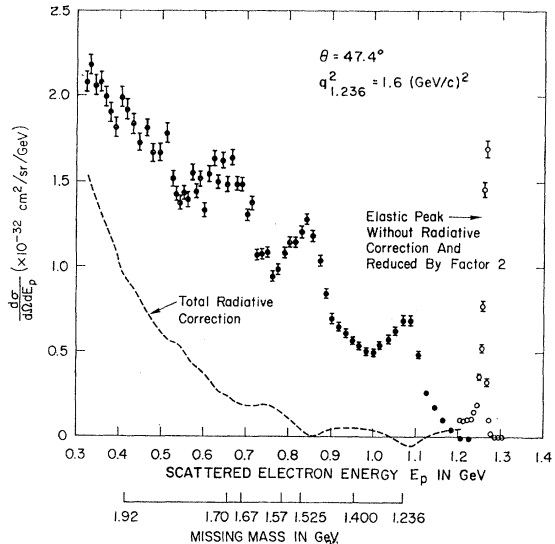


FIG. 1. A typical spectrum of inelastic ep scattering and the radiative corrections. Both of these curves are taken directly from Brasse *et al.* (Ref. 4).

corrections to muon scatterings. In Sec. III we calculate the elastic radiative tail using our exact formula [Eq. (B5)] and several versions of approximation formulas. We conclude that all different versions of approximation formulas are good near the peak but predict result in error by 30 to 40% when the electron loses more than $\frac{1}{3}$ of its energy through bremsstrahlung. Hence it is essential to use the exact formula to calculate the elastic radiative tail, which is usually the most dominant background to the inelastic electron scattering. Fortunately, it is rather easy to apply the exact formula to calculate the elastic radiative tail. For the continuum part of the spectrum, after elastic radiative tails have been subtracted, one is essentially forced to use an approximation formula. This is because our exact formula [Eq. (B6)] for the continuous spectra can be used only if the two *inelastic* form factors $F(q^2, M_f^2)$ and $G(q^2, M_f^2)$ have been separated out of the data. This is impossible before one applies the radiative corrections to the data. However, we believe the approximation formula is quite adequate for handling the radiative corrections to the continuous part of the spectrum. This optimism is based on the results given in Table III and Table IV in which we have compared the radiative tails of the elastic peak and the 3-3 resonance using both the exact formula and various approximation formulae. In Sec. IV, we treat the radiative corrections to the continuous spectrum, using the 3-3 resonance as an example. We first calculate the nonradiative 3-3 cross section using the method described by Dufner and Tsai¹⁶ and then include the effects due to straggling and radiative corrections. We give a procedure to extract the nonradiative cross section from the experimental data; this is called an "unfolding procedure." When the target particle is an

electron or a muon, both nonradiative and radiative cross sections are calculable, hence it is never necessary to consider the unfolding procedure. In contrast when the target is a proton or a nucleus, there is no reliable theory of strong interaction to give a theoretical nonradiative cross section; hence it is necessary to extract the nonradiative cross sections from the radiative (i.e., experimental) cross sections. In Sec. IV.B we show in great detail how this can be accomplished. Examples of the results of unfolding the inelastic-electron spectra are given using the experimental data obtained by the experimental group at the Stanford Linear Accelerator Center. We emphasize that experiments have to be planned carefully before its execution so that the radiative corrections can be applied. We suggest several items which are useful for the design of the experiments. In Sec. V, our results are discussed and summarized.

For convenience we have called our target particle a proton, but it is obvious that the treatment given in this paper is applicable to any nucleus as long as its atomic number, Z , is small compared with $\alpha^{-1}=137$. Our formulas are applicable for incident electron energies down to a few million electron volts with the exception of our straggling formula, Eq. (A.3). The latter becomes inaccurate when the electron energy is less than ~ 100 MeV due to our use of the complete screening formula for bremsstrahlung and neglect of the contribution from the ionization effect.

The notations used in this paper (except in Sec. II) are summarized below for easy reference. We use the convention $\hbar=c=1$. Energy and momentum are always in gigaelectron volts. The metric used is such that $ps=E_p E_p - \mathbf{p} \cdot \mathbf{s}$:

- $s=(E_s, \mathbf{s})$: four momentum of the incident electron;
- $p=(E_p, \mathbf{p})$: four momentum of the outgoing electron;
- $p_i=(M, 0)$: four momentum of the target particle;
- $k=(\omega, \mathbf{k})$: four momentum of the real photon emitted;
- $p_f=s+p_i-p-k$: four momentum of the final hadronic system;
- $u=(u_0, \mathbf{u}) \equiv s+p_i-p=p_f+k$;
- $(u^2)^{1/2}=[(p_f+k)^2]^{1/2}$: missing mass;
- $q^2=(s-p-k)^2=(p_f-p_i)^2$;
- M, M_f, m, m_μ, m_π : masses of target particle, final hadronic system, electron, muon, and pion, respectively;
- $M_{33}=1.236$ GeV, $M_p=0.938$ GeV;
- θ : scattering angle of the electron;
- θ_k : angle between \mathbf{u} and \mathbf{k} ;
- θ_s : angle between \mathbf{u} and \mathbf{s} ;
- θ_p : angle between \mathbf{u} and \mathbf{p} ;
- T : target thickness in unit of radiation length;
- t_{iw}, t_{fw} : initial and final target window thicknesses in unit of radiation length;
- Z : atomic number of the target nucleus;

A : atomic weight of the target nucleus;
 $N: 6.023 \times 10^{23}$ = Avogadro's number;
 $r_0: 2.818 \times 10^{-13}$ cm, classical radius of the electron.

The reader is advised to read the Appendices first before reading the text.

A review paper on the same subject by L. M. Maximon appears previous to this one in this issue. Although written in different spirits, the two papers complement each other in many places. While Maximon's paper explains the basic terminology of radiative corrections and gives a guide to the literature on the subject, our paper gives a detailed description of a workable procedure for actually handling the experimental data. A few questions of terminology and apparently conflicting statements in the two papers warrant clarification. At the end of Sec. 2, Maximon says that a fundamental shortcoming of the peaking approximation is its inability to go smoothly into the radiative correction proper. We show a way that this defect can easily be corrected, as can be seen by comparing our Eq. (C.8) with the Δ -dependent part of our Eq. (B.7). In our opinion, the real trouble with the peaking approximation is that it is not easy to improve it so that it reproduces the correct result for a hard-photon emission independent of the behavior of the form factors. In Maximon's terminology, the first term in our Eq. (IV.1) is called the "radiative correction" and the two remaining integrals in that equation are called either the "hard-photon contribution" or the "contribution from the radiative tail" of the lower-mass states of the final target system. We adopted the usual convention and used the word "radiative corrections" for the entire procedure. We have completely ignored the so-called dispersive effects, i.e., the real part of the two-photon exchange contribution mentioned at the end of Maximon's paper. The reason is that these calculations are highly dependent upon the detailed mechanism of strong interactions; hence they should be treated separately from the part of the radiative corrections which is dominant and relatively independent of the strong-interaction mechanism. This effect is very interesting from the theoretical point of view because it is so model dependent. The effect can be measured experimentally by comparing the e^+ and e^- scattering using the same target.

II. RADIATIVE CORRECTIONS TO THE ELASTIC PEAK

Radiative corrections to the elastic peak is a very well-known subject, hence we shall discuss only those points which have practical interest.

Schwinger¹⁷ first calculated the radiative corrections for *potential scattering* and found that the measured cross section (meas) should be related to the lowest-order cross section (Born) by a factor $(1+\delta)$:

$$d\sigma/d\Omega|_{\text{meas}} = (1+\delta)(d\sigma/d\Omega)|_{\text{Born}}, \quad (\text{II.1})$$

where

$$\begin{aligned} \delta = & \frac{-2\alpha}{\pi} \left\{ \left(\ln \frac{E}{\Delta E} - \frac{13}{12} \right) \ln \frac{-q^2}{m^2} - 1 \right\} \\ & + \frac{17}{36} + \frac{1}{2} f(\theta) \}, \\ (\theta) = & \ln (\sin^2 \frac{1}{2}\theta) \ln (\cos^2 \frac{1}{2}\theta) + \Phi(-\sin^2 \frac{1}{2}\theta). \end{aligned} \quad (\text{II.2})$$

Here q is the four-momentum transfer, E is the energy of incident or scattered electrons (in *potential scattering* they are identical), and ΔE is the maximum energy loss of the electron or the maximum energy of the photon allowed by kinematics (they are identical in *potential scattering*). Schwinger also noticed that when $\Delta E \rightarrow 0$, δ in Eq. (II.2) becomes negatively infinite, whereas on physical grounds, $d\sigma/d\Omega|_{\text{meas}}$ should go to zero as $\Delta E \rightarrow 0$. This is due to the fact that the multiple photon emissions have been neglected, and he conjectured that $(1+\delta)$ in Eq. (II.1) should be replaced by e^δ if higher-order radiative corrections are taken into account. Later Yennie and Suura¹⁸ and Yennie, Frautschi, and Suura¹⁹ proved that indeed the infrared divergent part of δ in Eq. (II.1),

$$\delta_{\text{inf}} = (-2\alpha/\pi)[\ln(-q^2/m^2) - 1] \ln(E/\Delta E), \quad (\text{II.3})$$

should be exponentiated (i.e., $1+\delta_{\text{inf}} \rightarrow e^{\delta_{\text{inf}}}$). As far as we know it is still an open question whether other contributions to δ , $\delta_{\text{vertex}} + \delta_{\text{vac}} = \delta - \delta_{\text{inf}}$, should be exponentiated or should assume some entirely different form such as $1+\delta_{\text{vertex}}+\delta_{\text{vac}}-(1-\delta_{\text{vertex}}-\delta_{\text{vac}})^{-1}$.

However, for practical applications this is an academic question at the presently available energies because δ_{vac} and δ_{vertex} are given by

$$\delta_{\text{vac}} = (2\alpha/\pi)[(-5/9) + \frac{1}{3} \ln(-q^2/m^2)] \quad (\text{II.4})$$

and

$$\delta_{\text{vertex}} = (2\alpha/\pi)[-1 + \frac{3}{4} \ln(-q^2/m^2)], \quad (\text{II.5})$$

respectively. Even if $-q^2=20$ GeV 2 , we have $\delta_{\text{vac}}=2.58 \times 10^{-2}$, $\delta_{\text{vertex}}=5.9 \times 10^{-2}$. Hence $(\delta_{\text{vac}}+\delta_{\text{vertex}})^2$ contributes at most 0.7%. In contrast to this the exponentiation of δ_{inf} is absolutely essential at high energies and at large momentum transfers because ΔE must be taken small enough to avoid the pion threshold, resulting in a magnitude for δ_{inf} very close to -1 .

When the momentum transfer $| -q^2 |^{1/2}$ becomes larger than or comparable to the mass of the target particle, we have to take into account both the kinematical effect due to target recoil and the dynamical effect due to photon emission by the target system. Neither of these effects is contained in Eq. (II.2).

The expression for δ containing these two effects was first given by Tsai¹⁴ (T) and later by Meister

and Yennie (MY).¹⁵ Tsai's expression can be written as

$$\delta = \frac{-\alpha}{\pi} \left(\frac{2}{9} - \frac{1}{6} \ln \left(\frac{-q^2}{m^2} \right) + \left(\ln \frac{-q^2}{m^2} - 1 + 2Z \ln \eta \right) \left(2 \ln \frac{E_1}{\Delta E} - 3 \ln \eta \right) - \Phi \left(\frac{E_3 - E_1}{E_3} \right) - Z^2 \ln \frac{E_4}{M} \right. \\ \left. + Z^2 \ln \frac{M}{\eta \Delta E} \left(\frac{1}{\beta_4} \ln \frac{1+\beta_4}{1-\beta_4} - 2 \right) + \frac{Z^2}{\beta_4} \left\{ \frac{1}{2} \ln \frac{1+\beta_4}{1-\beta_4} \ln \frac{E_4+M}{2M} - \Phi \left[- \left(\frac{E_4-M}{E_4+M} \right)^{1/2} \left(\frac{1+\beta_4}{1-\beta_4} \right)^{1/2} \right] \right\} \right. \\ \left. + Z \left[\Phi \left(- \frac{M-E_3}{E_1} \right) - \Phi \left(\frac{M(M-E_3)}{2E_3E_4-ME_1} \right) + \Phi \left(\frac{2E_3(M-E_3)}{2E_3E_4-ME_1} \right) + \ln \left| \frac{2E_3E_4-ME_1}{E_1(M-2E_3)} \right| \ln \left(\frac{M}{2F_3} \right) \right] \right. \\ \left. - Z \left[\Phi \left(- \frac{E_4-E_3}{E_3} \right) - \Phi \left(\frac{M(E_4-E_3)}{2E_1E_4-ME_3} \right) + \Phi \left(\frac{2E_1(E_4-E_3)}{2E_1E_4-ME_3} \right) + \ln \left| \frac{2E_1E_4-ME_3}{E_3(M-2E_1)} \right| \ln \left(\frac{M}{2E_1} \right) \right] \right. \\ \left. - Z \left[\Phi \left(- \frac{M-E_1}{E_1} \right) - \Phi \left(\frac{M-E_1}{E_1} \right) + \Phi \left(\frac{2(M-E_1)}{M} \right) + \ln \left| \frac{M}{2E_1-M} \right| \ln \left(\frac{M}{2E_1} \right) \right] \right. \\ \left. + Z \left[\Phi \left(- \frac{M-E_3}{E_3} \right) - \Phi \left(\frac{M-E_3}{E_3} \right) + \Phi \left(\frac{2(M-E_3)}{M} \right) + \ln \left| \frac{M}{2E_3-M} \right| \ln \left(\frac{M}{2E_3} \right) \right] \right) \\ - \frac{\alpha}{\pi} \left(-\Phi \left(\frac{E_1-E_3}{E_1} \right) + \frac{Z^2}{\beta_4} \left\{ \Phi \left[\left(\frac{E_4-M}{E_4+M} \right)^{1/2} \left(\frac{1-\beta_4}{1+\beta_4} \right)^{1/2} \right] - \Phi \left[\left(\frac{E_4-M}{E_4+M} \right)^{1/2} \right] + \Phi \left[- \left(\frac{E_4-M}{E_4+M} \right)^{1/2} \right] \right\} \right). \quad (\text{II.6})$$

The last four Spence functions in the second set of heavy parenthesis were ignored in the original paper of Tsai¹⁴ because they are always small when $Z=1$. These terms are reinserted here so that the formula gives a correct limit when Z is large. Meister and Yennie's formula is

$$\delta = \frac{\alpha}{\pi} \left\{ \left[\ln \left(\frac{2p_1p_3}{m^2} \right) - 1 \right] \ln \left[\eta \left(\frac{\Delta E_3}{E_3} \right)^2 \right] + \frac{1}{6} \ln \left(\frac{2p_1p_3}{m^2} \right) - \frac{1}{2} \ln^2 \eta - \frac{2}{9} \right\} \\ + \frac{Z\alpha}{\pi} \left\{ \ln \eta \ln \left[\eta \left(\frac{E_1}{E_4} \right)^2 \left(\frac{\Delta E_3}{E_3} \right)^4 \right] - \beta \left(\frac{2E_1}{M} \right) + \beta \left(\frac{2E_3}{M} \right) \right\} \\ + \frac{Z^2\alpha}{\pi} \left\{ \left[\frac{E_4}{p_4} \ln \left(\frac{E_4+p_4}{M} \right) - 1 \right] \ln \left[\frac{E_1^2}{ME_4} \left(\frac{\Delta E_3}{E_3} \right)^2 \right] + \frac{3}{2} \ln \left(\frac{2E_4}{M} \right) - \frac{1}{2} \ln^2 \left(\frac{E_4}{M} \right) \right\}. \quad (\text{II.7})$$

The notation used in both formulas is as follows: E_1 , E_3 , and E_4 are energies of incident electron, scattered electron, and the recoil nucleus, respectively. The masses of the electron and the target particle are m and M , respectively. The step function β is defined by MY as $\beta(x) = (\ln^2 x)\theta(1-x)$; β_4 is the velocity of the recoil particle in units of the velocity of light, $\eta = E_1/E_3$, and $\Delta E = \Delta E_3 = E_{3\text{ peak}} - E_{3\text{ min}}$ as was shown in Fig. 1 of Tsai's paper.¹⁴ Z is the atomic number of the target particle when the incident particle is e^- and the sign of Z is changed when the incident particle is e^+ , e.g., $Z=1$ for e^-p scattering and $Z=-1$ for e^+p scattering. $\Phi(x)$ is the Spence function²⁰ defined by

$$\Phi(x) = \int_0^x \frac{-\ln |1-y|}{y} dy. \quad (\text{II.8})$$

In Table I and Table II, we compare the numerical values given by Eqs. (II.6) and (II.7). We notice that for $e^\pm p$ scattering, these two formulas give practically identical results. When Z is high, Eq. (II.6) gives a reasonable answer, whereas Eq. (II.7) does not. Since there are some experimentally detectable differences in

the two formulas, it is important to know the origins of these differences. They are as follows:

(1) In MY all the Spence functions are approximated by logarithmic functions using the following relations²⁰:

$$\Phi(x) = x + \frac{1}{4}x^2 + \frac{1}{9}x^3 + \dots + (x^n/n^2) + \dots, \quad \text{if } |x| \leq 1;$$

$$\Phi(1) = \frac{1}{6}\pi^2 \quad \text{and} \quad \Phi(-1) = -\frac{1}{12}\pi^2;$$

for $x > 1$,

$$\Phi(x) = -\frac{1}{2} \ln^2 |x| + \frac{1}{3}\pi^2 - \Phi(1/x);$$

for $x < -1$,

$$\Phi(x) = -\frac{1}{2} \ln^2 |x| - \frac{1}{6}\pi^2 - \Phi(1/x).$$

The Spence function $\Phi(x)$ was subsequently approximated by $\Phi(x) = 0$ when $|x| < 1$, and $\Phi(x) = -\frac{1}{2} \ln^2 |x|$ when $|x| > 1$. We regard this approximation as rather inadequate because it can cause an error of $(\alpha/\pi)(\pi^2/3) \times (1, Z, Z^2) \approx 1\%$ in e^-p scattering for each Spence function used. Since there are more than a dozen Spence functions involved in the problem, the resultant error

TABLE I. Radiative corrections for e^-p and e^+p elastic scattering ($\Delta E_3/E_3 = 1\%$).

Incident electron energy (GeV)	Scattering angle (deg)	Scattered electron energy (GeV)	$-q^2$ (GeV/c) ²	A			Meister and Yennie		
				Tsai			Z^0 term	Z^1 term	Z^2 term
17.314	35.100	3.975	25.031	-0.2296	-0.0563	-0.0411	-0.2296	-0.0566	-0.0310
15.999	19.700	8.007	14.996	-0.2516	-0.0267	-0.0307	-0.2516	-0.0266	-0.0220
14.649	18.800	7.992	12.492	-0.2521	-0.0234	-0.0279	-0.2521	-0.0232	-0.0197
13.329	17.600	8.006	9.990	-0.2523	-0.0196	-0.0247	-0.2523	-0.0194	-0.0169
11.999	16.082	7.997	7.510	-0.2518	-0.0155	-0.0207	-0.2518	-0.0153	-0.0136
10.723	14.000	8.005	5.100	-0.2499	-0.0110	-0.0159	-0.2499	-0.0108	-0.0097
6.032	17.186	4.687	2.525	-0.2402	-0.0097	-0.0106	-0.2402	-0.0095	-0.0056
2.201	38.601	1.455	1.400	-0.2256	-0.0168	-0.0083	-0.2256	-0.0168	-0.0041
2.206	15.999	2.022	0.346	-0.2138	-0.0035	-0.0022	-0.2138	-0.0034	0.0008

Incident electron energy (GeV)	Scattering angle (deg)	Scattered electron energy (GeV)	$-q^2$ (GeV/c) ²	B			e^-p elastic scattering			e^+p elastic scattering		
				e^-p elastic scattering			δ_1 (by Tsai)	δ_2 (by Meister and Yennie)	$\delta_1 - \delta_2$	δ_1 (by Tsai)	δ_2 (by Meister and Yennie)	$\delta_1 - \delta_2$
17.314	35.100	3.975	25.031	-0.3271	-0.3173	0.0100	-0.2144	-0.2041	-0.0103	-0.2556	-0.2469	-0.0087
15.999	19.700	8.007	14.996	-0.3090	-0.3002	0.0088	-0.2567	-0.2485	-0.0082	-0.2574	-0.2498	-0.0076
14.649	18.800	7.992	12.492	-0.3034	-0.2950	0.0084	-0.2570	-0.2501	-0.0069	-0.2548	-0.2487	-0.0061
13.329	17.600	8.006	9.990	-0.2965	-0.2886	-0.0079	-0.2411	-0.2363	-0.0048	-0.2411	-0.2363	-0.0048
11.999	16.082	7.997	7.510	-0.2880	-0.2807	-0.0073	-0.2171	-0.2129	-0.0042	-0.2171	-0.2129	-0.0042
10.723	14.000	8.005	5.100	-0.2769	-0.2704	-0.0065	-0.2125	-0.2096	-0.0029	-0.2125	-0.2096	-0.0029
6.032	17.186	4.687	2.525	-0.2606	-0.2553	-0.0053	-0.2171	-0.2129	-0.0042	-0.2171	-0.2129	-0.0042
2.201	38.601	1.455	1.400	-0.2507	-0.2465	-0.0042	-0.2125	-0.2096	-0.0029	-0.2125	-0.2096	-0.0029
2.206	15.999	2.022	0.346	-0.2195	-0.2164	-0.0031	-0.2125	-0.2096	-0.0029	-0.2125	-0.2096	-0.0029

^a We wish to thank Dr. R. W. Brown for pointing out the numerical mistakes in this column which we made in our original manuscript.

is difficult to estimate. We are unable to determine for the MY calculation how much this approximation contributes to the difference in the numerical values given in Table I. This approximation is especially bad when Z is large as can be seen from Table II, where we have calculated the radiative corrections to $e^\pm + {}^{48}\text{Ca}$ elastic scattering. In any large-scale data analysis, one has to use a computer anyway and the Spence function $\Phi(x)$ defined by Eq. (II.8) is no more difficult to obtain than the logarithmic function when a computer is used.

(2) Another source of the difference between T and MY is in the manner in which the two-photon exchange diagrams are handled in the two papers. Neither of these papers claims to have treated the two-photon exchange terms completely, because the effects of strong interactions to these diagrams were ignored. These authors were forced to consider these diagrams because they are needed to supply terms to cancel the infrared divergence in real photon emission. In T, only the infrared terms were extracted from these diagrams, whereas in MY additional terms called spin-convection terms were also extracted. In practice, the radiative correction δ is used for two purposes: (a) to obtain nucleon form factors and (b) to obtain the contribution of the real part of the two-photon exchange²¹ diagrams by comparing e^+p and e^-p scatterings. Strictly speaking (b) has to be done before (a). But usually it is assumed that after applying the radiative corrections, the re-

mainder of the two-photon contribution is small. For the purpose of (a), one method of extraction cannot be preferred over the other, because one does not know which method represents more closely the bulk of two-photon exchange contributions until the difference in e^+p and e^-p cross sections are measured experimentally. For the purpose of (b), the question of preference of one method over the other is just a matter of convenience in the theoretical analysis. Suppose one wants to use a certain theory of strong interactions to understand the two-photon exchange process by comparing his theory to the difference in e^-p and e^+p cross sections. Then, whether the method of T or of MY is used, one must restore the part which each has subtracted from these diagrams before the comparison can be made. The method of T is somewhat simpler than that of MY because in T only a simple, well-defined analytical function called

$$k(p_i, p_j) \equiv (p_i p_j) \int_0^1 \frac{dy}{p_y^2} \ln \frac{p_y^2}{\lambda^2}$$

$$[\text{where } p_y = p_i y + (1-y)p_j]$$

was extracted from each diagram, whereas in MY a more complicated procedure was used to extract the contribution from two-photon exchange diagrams (hence it requires more work to put back what MY have subtracted from these diagrams). The reason T extracted only $k(p_i, p_j)$'s from the two-photon exchange dia-

TABLE II. Radiative corrections for e^- - ^{48}Ca elastic scattering ($\Delta E_3/E_3 = 1\%$).

Incident electron energy (GeV)	Scattering angle (deg)	Scattered electron energy (GeV)	Tsai			Meister and Yennie		
			\bar{Z}^0 term	Z^1 term	Z^2 term	Z^0 term	Z^1 term	Z^2 term
0.50	30	0.4993	0.0669	-0.1895	-0.0015	-0.0002	-0.1912	-0.0014
0.50	60	0.4972	0.2486	-0.2109	-0.0054	-0.0007	-0.2170	-0.0051
0.50	90	0.4945	0.4945	-0.2220	-0.0108	-0.0014	-0.2341	-0.0101
0.50	120	0.4918	0.7377	-0.2283	-0.0161	-0.0021	-0.2465	-0.0152

grams was not only for simplicity. In addition it was found that in the exact calculation of radiative corrections to $e-e$ scattering,²² the remainder is indeed very small after the $k(p_i, p_f)$'s were subtracted (it, at most, contributes 0.1% to the cross section and is independent of energy in the c.m. system). It is a puzzle then why the spin-convection terms do not make much of a contribution to the $e-e$ scattering. The exact two-photon exchange contribution to $e\mu$ scattering has been computed by Erickson.²³ The contributions of these diagrams to the cross section after subtracting the $k(p_i, p_f)$'s are given in Eqs. (51)–(55) of Erickson's paper.²³ It would be interesting to compare Erickson's results with MY's spin convection contributions. These remarks are important when one wants to compare the difference in e^+p and e^-p scatterings with some model of strong interaction in two-photon exchange interaction.

The effect of straggling in the target system can be incorporated into the radiative corrections in the following way:

$$d\sigma/d\Omega|_{\text{meas}} = d\sigma/d\Omega|_{\text{Rosenbluth}} \exp(\delta + \delta_t),$$

where

$$\delta_t = -\{[b_w t_{iw} + \frac{1}{2} b T] \ln(E_1/\eta^2 \Delta E) + [b_w t_{fw} + \frac{1}{2} b T] \ln(E_3/\Delta E)\}; \quad (\text{II.9})$$

T , t_{iw} , and t_{fw} are the target, the initial window, and the final window thicknesses, respectively, in units of radiation length. The coefficients b_w and b are very close to 4/3, and their exact numerical values depend upon Z of the material as given by Eq. (A.4) in Appendix A.

For elastic scattering of muons, δ_t can be taken to be zero because the muon bremsstrahlung in the target is reduced by a factor of $(m_e/m_\mu)^2 \approx 1/40\,000$ compared with electrons. If the muon mass is small compared with its energy and momentum transfer, then the formulas given by T or MY may be used for δ , provided m is replaced by m_μ and the vacuum polarization due to the electron pair in the bubble, Eq. (II.4), is added to the expression. The order of magnitude of the ratio of muon radiative corrections to the electron radiative corrections is roughly given by $(\ln(-q^2/m_\mu^2) - 1) \times (\ln(-q^2/m^2) - 1)^{-1}$. It is equal to ≈ 0.25 when $-q^2 = 1 \text{ BeV}^2$. This statement is also roughly correct for the radiative tails, as will be shown in Sec. V and Fig. 5. Similar observation concerning the radiative corrections to muon scattering has been made by Maximon and Tzara.³⁴

III. ELASTIC RADIATIVE TAIL AND VALIDITY OF VARIOUS APPROXIMATION FORMULAS

A. Radiative Tail from the Elastic Peak

After the elastic form factors $G_e(q^2)$ and $G_m(q^2)$ are obtained from the experiments, one can calculate the radiative tail due to the elastic peak and immediately

TABLE III. Radiative tails from elastic $e\bar{p}$ scattering.

E_p (GeV)	Missing Mass (u^2) $^{1/2}$ GeV	Exact	Mo and Tsai	Hand	Allton- Bjorken	Equivalent radiators
$E_s = 20 \text{ GeV}, \theta = 5^\circ, E_{p \max} = 18.499 \text{ GeV}, \frac{d\sigma_0}{d\Omega} = 22 \times 10^{-33} \text{ cm}^2/\text{sr}$ $10^{-33} \text{ cm}^2/\text{GeV}/\text{sr}$						
18.4	1.040	15.85	15.85	15.85	15.85	15.85
17.5	1.705	1.884	1.860	1.861	1.860	1.862
16.5	2.222	1.246	1.176	1.179	1.175	1.179
10.0	4.257	5.011	3.562	3.863	3.518	3.835
5.0	5.317	42.70	34.59	44.16	33.34	42.03
1.5	5.947	581.9	506.5	788.2	474.7	676.5
$E_s = 5 \text{ GeV}, \theta = 5^\circ, E_{p \max} = 4.901 \text{ GeV}, \frac{d\sigma_0}{d\Omega} = 29.6 \times 10^{-30} \text{ cm}^2/\text{sr}$ $10^{-30} \text{ cm}^2/\text{GeV}/\text{sr}$						
4.8	1.036	17.26	17.26	17.26	17.26	17.26
4.5	1.283	4.533	4.523	4.532	4.522	4.526
4.0	1.614	2.250	2.228	2.252	2.225	2.236
2.5	2.340	1.665	1.561	1.732	1.536	1.615
1.0	2.889	5.69	4.918	6.967	4.656	5.226
$E_s = 1 \text{ GeV}, \theta = 5^\circ, E_{p \max} = 0.996 \text{ GeV}, \frac{d\sigma_0}{d\Omega} = 1.38 \times 10^{-27} \text{ cm}^2/\text{sr}$ $10^{-27} \text{ cm}^2/\text{GeV}/\text{sr}$						
0.98	0.954	3.733	3.733	3.733	3.733	3.733
0.90	1.030	0.6244	0.6233	0.6255	0.6239	0.6239
0.70	1.199	0.2275	0.2228	0.2322	0.2213	0.2247
0.50	1.347	0.1934	0.1806	0.2079	0.1765	0.1846
0.30	1.480	0.3048	0.2655	0.3672	0.2516	0.3080
0.20	1.543	0.5435	0.4636	0.7304	0.4292	0.5612

subtract its contribution from the inelastic spectrum. We would like to emphasize that the peaking approximation to the radiative tail from the elastic peak can be in error by as much as 30 to 40% when the energy of the scattered electron is $E_p < \frac{1}{3}E_{p \max}$. Hence the result of the exact calculation given in the Appendix B must be used when the energy loss is large. The formulas needed for calculating the radiative tail due to the elastic peak in the deep inelastic region are given by the sum of Eq. (A.16) and Eq. (B.5):

$$\frac{d\sigma_{0,\text{tot}}}{d\Omega dE_p}(E_s, E_p, T) = \frac{d\sigma_{0,i}(E_s, E_p, T)}{d\Omega dE_p} + \frac{d\sigma_{0,r}(E_s, E_p)}{d\Omega dE_p}, \quad (\text{III.1})$$

where the first term is due to straggling in the target, and its explicit expression is given by Eq. (A.16); the second term is due to the internal bremsstrahlung, and its lowest-order exact expression is given by Eq. (B.5) [our G_0 and F_0 are related to G_e and G_m by Eqs. (III.2) and (III.3)]. For calculating the radiative tail near the elastic peak such as at the pion threshold, it is necessary to take into account the multiple photon emission which is ignored in Eq. (B.5). As will be shown in the next section, all versions of approximate formulas give excellent results near the elastic peak compared with the exact lowest-order result. Furthermore, the effect of multiple photon emission is easy to take into account if the approximate formulas are used. Hence the easiest way to calculate the radiative tail near the elastic peak is to ignore the second term in

the right-hand side of Eq. (III.1) and add an equivalent radiator thickness, $t_r = (\alpha/b\pi)[\ln(2sp/m^2) - 1]$, to $T/2$ in Eq. (A.16). The factor $[\ln(E_0/E)]^{bt}$ in Eq. (A.3) automatically takes into account the effect of the multiple photon emission.

B. Comparisons of Various Versions of Peaking Approximations with the Exact Formula

In contrast to the radiative tail from the elastic peak, it is not easy to apply the exact formula to calculate the radiative corrections to the continuous spectrum because the form factors $F(q^2, M_f^2)$ and $G(q^2, M_f^2)$ have to be separated out before we can apply the exact formula, Eq. (B.8). Hence one is essentially forced to use an approximation formula (which requires only the knowledge of cross sections) to calculate the radiative corrections to the continuum part of the spectrum after the elastic radiative tail has been subtracted from the inelastic-electron spectrum. Therefore, in this section we investigate the reliability of various approximation formulas.

In Table III, results are given for the radiative tail of the $e\bar{p}$ elastic peak calculated according to the exact formula Eq. (B.5) and also several versions of approximations including our own Eq. (C.11). In Table IV results are given for the radiative tails from the 3-3 resonance using (a) the exact formula Eq. (B.5), (b) our version of the peaking approximation, Eq. (C.11), and (c) the method of equivalent radiators.

The elastic form factors of the proton used in the

calculation are [see Eq. (B.3)]

$$F_0(q^2) = 4(G_e^2 + \tau G_m^2)/(1 + \tau), \quad (\text{III.2})$$

$$G_0(q^2) = -q^2 G_m^2, \quad (\text{III.3})$$

$$\tau = -q^2/4M_p^2,$$

and²⁴

$$G_e = G_m/2.793 = [1 - (q^2/0.71 \text{ GeV}^2)]^{-2}. \quad (\text{III.4})$$

For the form factors associated with $e+p \rightarrow e+N^*$ (1236 MeV) a convenient parametrization valid in the range $0.1 \text{ GeV}^2 < -q^2 < 2.4 \text{ GeV}^2$ has been given by Dufner and Tsai¹⁶ assuming a pure $M1$ transition. In terms of our $F(q^2, M_f^2)$ and $G(q^2, M_f^2)$ defined by Eq. (B.1), Eq. (3.14) of Ref. 16 can be written as

$$F(q^2, M_f^2) = (2/M_p) G_2(q^2, M_f^2), \quad (\text{III.5})$$

$$G(q^2, M_f^2) = 2M_p G_1(q^2, M_f^2), \quad (\text{III.6})$$

where

$$\begin{aligned} G_1(q^2, M_f^2) &= (Q^2/-q^2) G_2(q^2, M_f^2) \\ &= \frac{\Gamma M_{33} M_f \pi^{-1}}{(M_f^2 - M_{33}^2)^2 + \Gamma^2 M_{33}^2} Q^{*2} 2C_3^2(q^2) \\ &\quad \frac{E_i^* + M_p}{3M_p}, \\ Q^2 &= (M_f^2 - q^2 - M_p^2)^2 (2M_p)^{-2} - q^2, \\ Q^{*2} &= M_p^2 Q^2 / M_f^2, \\ E_i^* &= (M_f^2 + M_p^2 - q^2) / (2M_f), \\ M_{33} &= 1.236 \text{ GeV}, \quad (\text{III.7}) \\ \Gamma(M_f^2) &= 0.1293 \text{ GeV} \frac{[0.85(p^*/m_\pi)]^3}{1 + [0.85(p^*/m_\pi)]^2}, \\ p^{*2} &= [(M_f^2 - M_p^2 + m_\pi^2)/(2M_f)]^2 - m_\pi^2, \quad (\text{III.8}) \\ [C_3(q^2) M_p]^2 &= 2.05^2 \exp[-6.3(-q^2)^{1/2}] [1 + 9.0(-q^2)^{1/2}] \quad (\text{III.9}) \end{aligned}$$

and where energy is in gigaelectron volts.

In this section we are interested only in investigating the validity of various versions of the approximation methods, hence we shall ignore the width Γ and replace the Breit-Wigner formula in Eq. (III.7) by a δ function (we restore the width in the next section)

$$\delta(M_f^2 - M_{33}^2) \leftarrow \Gamma M_{33} \pi^{-1} / [(M_f^2 - M_{33}^2)^2 + \Gamma^2 M_{33}^2]. \quad (\text{III.10})$$

Since the width of the N^* is neglected, we can use Eq. (B.5) for the exact calculation of the radiative tail from the 3-3 resonance and Eqs. (C.11), (C.8), and (B.3) for its peaking approximation. In the zero-width approximation, the form factors $F_j(q^2)$ and $G_j(q^2)$ which appear in Eqs. (B.5) and (B.3) can now be written as

$$\begin{aligned} G_j(q^2) &= M_p^2 (Q^2/-q^2) F_j(q^2) \\ &= \frac{4}{3} M_{33} (E_i^* + M_p) Q^{*2} C_3^2(q^2). \quad (\text{III.11}) \end{aligned}$$

In Table III we give numerical examples of the radiative tails from the elastic peak at $\theta=5^\circ$, $E_s=20$, 5, and 1 GeV. The third column labeled "exact" is based on Eq. (B.5). The fourth column labeled "Mo and Tsai" is based on our own peaking approximation, Eq. (C.11) of Appendix C. The fifth column labeled "Hand" is based on the peaking approximation formula of Hand,²⁵ which in the notation of our Appendix C [see Eqs. (C.7), (C.8), and (C.11)] can be written as

$$t_{s,p} = \frac{\alpha}{\pi} \left[x_{s,p} \left(\ln \frac{2sp}{m^2} - 1 \right) + \frac{1}{2} (1 - x_{s,p})^2 \ln \frac{4E_{s,p}^2}{m^2} \right] \quad (\text{Hand}). \quad (\text{III.12})$$

The sixth column labeled "Allton and Bjorken" is based on the peaking approximation formula of Allton⁷ and Bjorken,⁸ which in our notation can be written as

$$t_{s,p} = \frac{\alpha}{\pi} \frac{1}{2} (1 + x_{s,p})^2 \left[\ln \frac{2sp}{m^2} - 1 \right] \quad (\text{Allton and Bjorken}). \quad (\text{III.13})$$

The seventh column labeled "Equivalent Radiators" is based on a semiempirical formula obtained by assuming that the effect of the internal bremsstrahlung on the elastic or inelastic electron scattering is equivalent to placing one radiator before the scattering and another radiator of the same thickness after the scatter-

TABLE IV. Radiative tails from 3-3 resonance (zero-width approximation).

E_p GeV	Missing Mass $(u^2)^{1/2}$ GeV	Exact	Mo and Tsai	Equivalent radiators
$E_s=20 \text{ GeV}$	$\theta=5^\circ$	$E_p \text{ max}=18.17 \text{ GeV}$		
		$d\sigma_{33}/d\Omega=16.1 \times 10^{-33} \text{ cm}^2/\text{sr}$		
		$10^{-33} \text{ cm}^2/\text{GeV}/\text{sr}$		
17.5	1.705	1.941	1.934	1.934
16.5	2.222	1.032	1.012	1.011
10.0	4.257	2.373	2.269	2.329
5.0	5.317	8.916	9.396	10.25
1.5	5.947	17.15	18.03	19.39
$E_s=5 \text{ GeV}$	$\theta=5^\circ$	$E_p \text{ max}=4.560 \text{ GeV}$		
		$d\sigma_{33}/d\Omega=8.59 \times 10^{-30} \text{ cm}^2/\text{sr}$		
		$10^{-30} \text{ cm}^2/\text{GeV}/\text{sr}$		
4.5	1.283	8.246	8.249	8.250
4.0	1.614	.8624	.8642	.8664
2.5	2.340	.2229	.2243	.2341
1.0	2.889	.1182	.1158	.1332
$E_s=1 \text{ GeV}$	$\theta=5^\circ$	$E_p \text{ max}=0.650 \text{ GeV}$		
		$d\sigma_{33}/d\Omega=1.97 \times 10^{-30} \text{ cm}^2/\text{sr}$		
		$10^{-30} \text{ cm}^2/\text{GeV}/\text{sr}$		
0.6	1.275	15.17	15.24	15.28
0.5	1.347	4.264	4.308	4.370
0.3	1.480	1.307	1.328	1.441
0.2	1.543	0.8596	0.8752	1.015

ing. The thickness of each radiator is equal to

$$t_r = b^{-1}(\alpha/\pi) [\ln(2sp/m^2) - 1], \quad (\text{III.14})$$

where b is a number very close to $4/3$ as given by Eq. (A.4). Comparing Eqs. (A.16) and (A.19) with Eqs. (III.14) and (C.11) and remembering the fact that in this subsection we are ignoring the multiple photon emission {hence $[\ln(E_0/E)]^{b_t}$ in Eq. (A.3) must be set equal to 1 just for the discussion in this section}, we obtain

$$t_{s,p} = (\alpha/\pi) [x_{s,p} + \frac{3}{4}(1-x_{s,p})^2] \{\ln[2(sp)/m^2] - 1\} \\ \text{(equivalent radiators).} \quad (\text{III.15})$$

In Table IV we give numerical examples of the radiative tails from the 3-3 resonance (zero-width approximation) under experimental conditions identical to those of Table III. We give at the top of Tables III and IV the peak energy $E_{p,\max}$, the nonradiative elastic cross sections $d\sigma_0/d\Omega$, and $d\sigma_{33}/d\Omega$ for the 3-3 excitation.

From Tables III and IV we observe the following:

(1) All approximation formulas given above are very good near the peaks; they are accurate to within 1% compared with the exact formula when $(E_{p,\max} - E_p)/E_{p,\max} < 0.05$. The approximation seems to work better at low rather than at high incident energies.

(2) At around $E_p \sim \frac{1}{2}E_{p,\max}$ the approximation formulas can have errors of more than 30% compared with the exact formulas for the radiative tails from the elastic peak. Hence when the inelastic spectrum is dominated by the radiative tail of the elastic peak, the exact formula must be used.

(3) The rise of the radiative tail near the lower-energy end of the spectrum is very prominent for the elastic radiative tail but not so prominent for the 3-3 radiative tail. The reason for the rise of the elastic radiative tail is that the electron energy becomes very small after a high-energy photon is emitted by the incident electron along its direction of motion. The resulting low-energy electron is then scattered by the nucleus with a large cross section. For the 3-3 resonance, there is the so-called threshold factor $[Q^{*2}]$ in Eq. (III.11) which makes the rise in the cross section at low incident energy relatively mild compared with

the elastic scattering. If this is true for all other inelastic events, then we have a happy situation in which the radiative tail from an inelastic event affects only its immediate neighborhood where the approximation formulas work very well. Another comforting feature is that the peaking approximation seems to work better for the 3-3 radiative tail than for the elastic radiative tail. Of course we can always check whether these nice features of the 3-3 resonance radiative tail are shared by other inelastic events after the inelastic form factors have been obtained (see Sec. IV.D).

(4) It is difficult to judge which version of the approximations is best for the treatment of the inelastic spectrum because the error in the approximation seems to depend upon the behavior of the form factors. For example, for the elastic radiative tail the method of equivalent radiators seems to give the best over-all agreement with the exact formula, whereas for the 3-3 radiative tail our version of the peaking approximation seems to give a better result. However, the difference is small, especially near the peak.

IV. RADIATIVE CORRECTIONS TO CONTINUOUS SPECTRA

After the elastic radiative tail has been subtracted from the inelastic spectrum, the radiative corrections must be applied to the continuous part of the spectrum. We use the 3-3 resonance formulas, Eqs. (III.5)–(III.9), to illustrate this procedure. Let us first consider a reverse problem: namely, given a nonradiative cross section $d\sigma/d\Omega dE_p$ for the 3-3 resonance, what is the resultant cross section $d\sigma_{t+r}/d\Omega dE_p$ when the straggling and the radiative corrections are included? In Sec. IV.B we consider a more practical problem; namely, given a set of values for the experimental cross section, $d\sigma_{t+r}/d\Omega dE_p$, what should one do to obtain the nonradiative cross section $d\sigma/d\Omega dE_p$?

A. Change of 3-3 Resonance Curve Due to Radiative Corrections

The nonradiative cross section for the 3-3 resonance is given by Eq. (B.1) with form factors given by Eqs. (III.5)–(III.9). Then as a result of the straggling of the electron in the target and the radiative corrections, the measured spectrum would be given by

$$\begin{aligned} \frac{d\sigma_{t+r}(E_s, E_p)}{d\Omega dE_p} &= \frac{d\sigma}{d\Omega dE_p}(E_s, E_p) \exp(\delta_t + \delta_r) \\ &+ \left(\frac{\Delta}{E_p}\right)^{(1/2)f_p} \int_{E_{s,\min}(E_p)}^{E_s - \Delta} \frac{dE'_s}{E'_s - E_s} \{t_s + (b_w t_{iw} + \frac{1}{2}bT)[x_s + \frac{3}{4}(1-x_s)^2]\} (\ln x_s^{-1})^{f_s} \frac{d\sigma}{d\Omega dE_p}(E'_s, E_p) \\ &+ \left(\frac{\Delta}{E_s}\right)^{(1/2)f_p} \int_{E_p + \Delta}^{E_{p,\max}(E_s)} \frac{dE'_p}{E'_p - E_p} \{t_p + (b_w t_{iw} + \frac{1}{2}bT)[x_p + \frac{3}{4}(1-x_p)^2]\} (\ln x_p^{-1})^{f_p} \frac{d\sigma}{d\Omega dE_p}(E_s, E'_p), \end{aligned} \quad (\text{IV.1})$$

where $d\sigma/d\Omega dE_p(E_s, E_p)$ is the nonradiative cross section [see Eqs. (B.1) and (III.5)–(III.9)]. The functions

$$\delta_t = - \left[\left(b_w t_{iw} + \frac{bT}{2} \right) \ln \frac{E_s}{\Delta} + \left[b_w t_{fw} + \frac{1}{2}(bT) \right] \ln \frac{E_p}{\Delta} \right] \quad [\text{see Eq. (A.21)}],$$

$$\delta_r = \frac{-\alpha}{\pi} \left[\frac{\frac{2}{9}s - \frac{1}{6}}{m^2} \ln \frac{2(sp)}{m^2} + \left(\ln \frac{E_s}{\Delta} + \ln \frac{E_p}{\Delta} \right) \left(\ln \frac{2(sp)}{m^2} - 1 \right) - \Phi \left(-\frac{E_s - E_p}{E_p} \right) - \Phi \left(\frac{E_s - E_p}{E_s} \right) \right] \quad [\text{see Eq. (B.7)}],$$

where T is the target thickness in radiation lengths, t_{iw} and t_{fw} are the initial and final window thicknesses in radiation lengths, and b and b_w are values of b for the target and window materials given by Eq. (A.4),

$$x_s = E'_s/E_s, \quad x_p = E_p/E'_p,$$

$$t_r = b^{-1}(\alpha/\pi) [\ln(2sp/m^2) - 1] \quad [\text{see Eq. (III.14)}],$$

$$f_s = bt_r + b_w t_{iw} + \frac{1}{2}bT, \quad f_p = bt_r + b_w t_{fw} + \frac{1}{2}bT,$$

$$t_{s,p} = (\alpha/\pi) \left[\frac{1}{2} (1 + x_{s,p})^2 \right] \ln [2(sp)/m^2] - x_{s,p} \quad [\text{see Eqs. (C.8) and (III.15)}],$$

$$E_{s \min}(E_p) = (m_\pi^2 + 2M_p m_\pi + 2M_p E_p) / [2M_p - 2E_p(1 - \cos\theta)] \quad [\text{see Eq. (A.18)}],$$

$$E_{p \max}(E_s) = (2M_p E_s - 2M_p m_\pi - m_\pi^2) / [2M_p + 2E_s(1 - \cos\theta)] \quad [\text{see Eq. (A.19)}].$$

The effect due to multiple photon emissions in the internal bremsstrahlung has been approximated by the inclusion of the term t_r in f_s and f_p and also the exponentiation of δ_r in the first term of Eq. (IV.1). Also, the factors in front of the integrals, $(\Delta/E_p)^{f_p}$ and $(\Delta/E_s)^{f_s}$, have been replaced by their square roots. This will reduce the error introduced by neglecting region IV as shown in Fig. 3. In addition, it will make Eq. (IV.1) relatively insensitive to different choices of Δ (see discussion at the end of Appendix A).

Three curves are shown in Fig. 2(a) through 2(c). They represent, respectively,

- (1) $d\sigma/d\Omega dE_p$, the nonradiative cross section using Eqs. (B.1) and (III.5)–(III.9);
- (2) $d\sigma_r/d\Omega dE_p$, the radiative cross section, Eq. (IV.1), neglecting the straggling, i.e., $T=t_{iw}=t_{fw}=0$;
- (3) $d\sigma_{t+r}/d\Omega dE_p$, the radiative cross section, Eq. (IV.1), with $T=0.02$ radiation lengths, $t_{iw}=t_{fw}=0.005$ radiation lengths, and $b=b_w=4/3$.

All three curves are calculated for the incident electron energy of $E_s=20$ GeV and $\theta=5^\circ$. We have used various values of Δ in our calculation and found that the answers are quite insensitive to Δ . For example, when the missing mass is equal to 1.236 GeV, for Δ equal to 10 and 15 MeV, the values of the cross section are 5.18×10^{-32} and 5.15×10^{-32} cm²/sr·GeV, respectively. If we had used Eq. (A.21) instead of Eq. (A.22), the difference between these two cross sections would have been 3%.

B. Procedure for Unfolding the Experimental Data

In the previous section, we have demonstrated how to calculate the radiative cross section from the nonradiative cross section. However, the reverse procedure of extracting the nonradiative cross section $d\sigma/d\Omega dE_p$ from the measured cross section $d\sigma_{t+r}/d\Omega dE_p$ is needed. A procedure for doing this can be inferred from Eq. (IV.1). To show this, we rewrite Eq. (IV.1) in the following form:

$$\begin{aligned} \frac{d\sigma}{d\Omega dE_p}(E_s, E_p) &= \frac{d\sigma_{t+r}(E_s, E_p)}{d\Omega dE_p} \exp[-(\delta_t + \delta_r)] - \exp(-\delta_t - \delta_r) \left(\frac{\Delta}{E_p} \right)^{f_p/2} \int_{E_{s \min}(E_p)}^{E_s - \Delta} \frac{dE'_s}{E_s - E'_s} \psi(x_s) \frac{d\sigma}{d\Omega dE_p}(E'_s, E_p) \\ &\quad - \exp(-\delta_t - \delta_r) \left(\frac{\Delta}{E_s} \right)^{f_s/2} \int_{E_p + \Delta}^{E_{p \max}(E_s)} \frac{dE'_p}{E'_p - E_p} \psi(x_p) \frac{d\sigma}{d\Omega dE_p}(E_s, E'_p), \quad (\text{IV.2}) \end{aligned}$$

where

$$\psi(x_s) = \{t_s + (b_w t_{iw} + \frac{1}{2}bT)[x_s + \frac{3}{4}(1-x_s)^2]\} (\ln 1/x_s)^{f_s},$$

$$\psi(x_p) = \{t_p + (b_w t_{fw} + \frac{1}{2}bT)[x_p + \frac{3}{4}(1-x_p)^2]\} (\ln 1/x_p)^{f_p}.$$

This equation implies that if the nonradiative cross sections $\sigma(E'_s, E'_p)$ are known for $E'_s < (E_s - \Delta)$ at constant E_p and $E'_p > (E_p + \Delta)$ at constant E_s , then the nonradiative cross section $\sigma(E_s, E_p)$ can be obtained immediately from the measured cross section,

$\sigma_{t+r}(E_s, E_p)$. The cross sections $\sigma[E'_s < E_{s \min}(E_p), E_p]$ and $\sigma[E_s, E'_p > E_{p \max}(E_s)]$ are equal to zero if the elastic radiative tails have already been subtracted from the measured cross section. Hence one can obtain the nonradiative cross section in the neighborhood

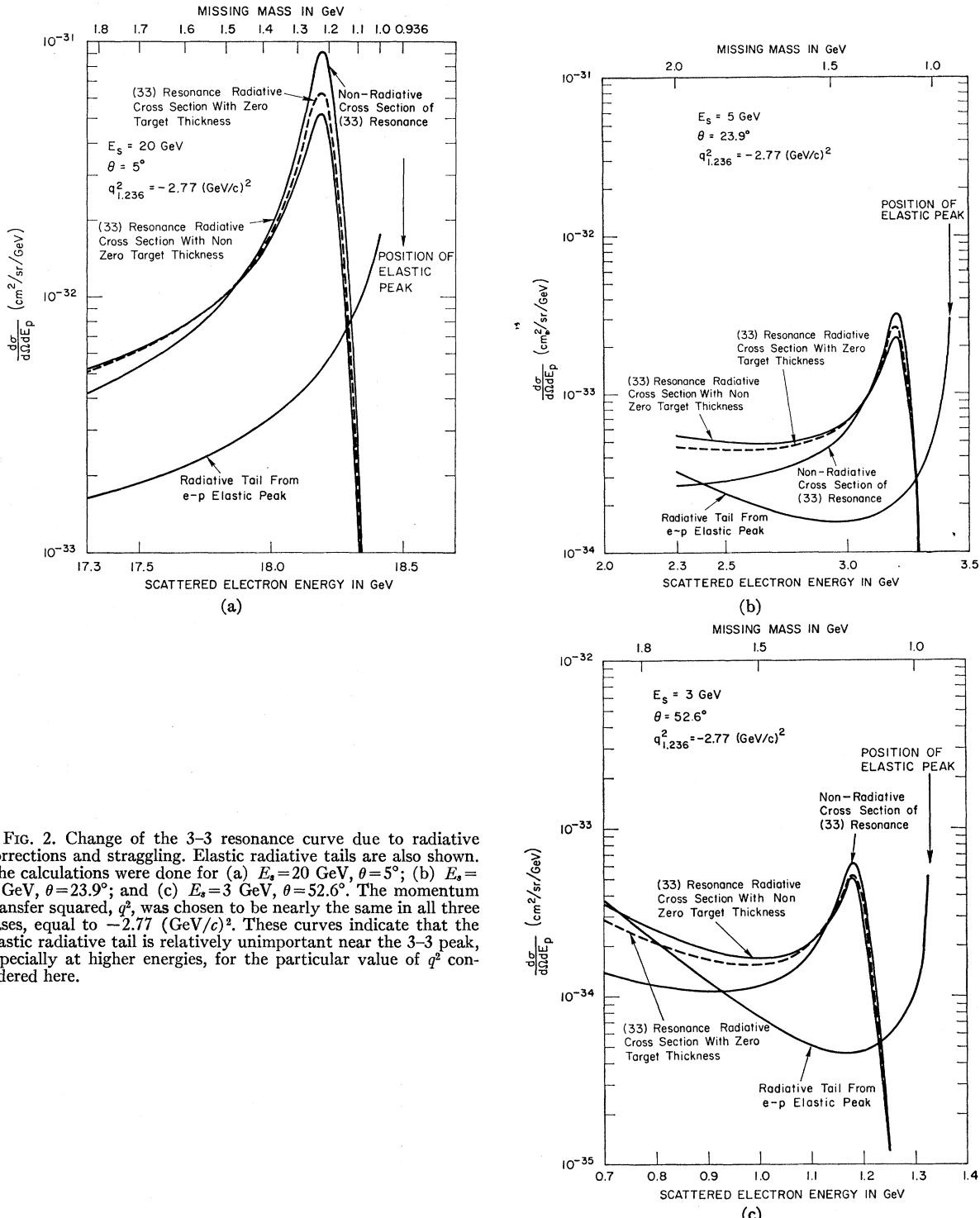


FIG. 2. Change of the 3-3 resonance curve due to radiative corrections and straggling. Elastic radiative tails are also shown. The calculations were done for (a) $E_s = 20$ GeV, $\theta = 5^\circ$; (b) $E_s = 5$ GeV, $\theta = 23.9^\circ$; and (c) $E_s = 3$ GeV, $\theta = 52.6^\circ$. The momentum transfer squared, q^2 , was chosen to be nearly the same in all three cases, equal to -2.77 $(\text{GeV}/c)^2$. These curves indicate that the elastic radiative tail is relatively unimportant near the 3-3 peak, especially at higher energies, for the particular value of q^2 considered here.

of the pion threshold along the line ab in Fig. 3. Knowing the cross sections on this strip, we can calculate the cross section for the next strip and so forth until we unfold the cross sections within the entire area abc in Fig. 3. There is no essential difficulty involved in

the procedure. The only thing one needs is an efficient computer program to handle the entire unfolding automatically. The best way to test the efficiency of this program is to do a reverse calculation of the previous section: namely, starting out with $\sigma_{t+r}(E_s, E_p)$ obtained

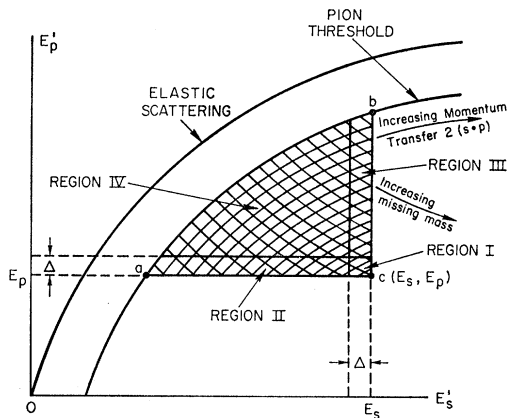


FIG. 3. Kinematic regions necessary for radiative corrections to inelastic electron scattering. E'_s is the incident electron energy and E'_p , the scattered electron energy.

from the previous section, try to reobtain the original cross section $\sigma(E_s, E_p)$. This exercise is extremely important in practical applications. It enables one to perfect the program for doing the radiative corrections without waiting for the experimental data. One can also get some feeling about the number of points measured inside the area abc in Fig. 3 that are needed to carry out the radiative corrections reliably. If one practices with enough examples of a similar nature, one may even be able to make an intelligent guess about the nonradiative cross section by just looking at the experimental data.

From the structure of Eq. (IV.2), the whole unfolding procedure should proceed smoothly as soon as we finish unfolding the first few points of data near the pion threshold. These first few points may be treated very crudely because the cross section near the pion threshold is very small and the error in these points will not significantly affect the unfolding of the subsequent points (the radiative tail of a small cross section is small). Let us first consider the radiative corrections to the first few points on each spectrum nearest to the pion threshold as shown in Fig. 4. We have assumed that there are four spectra available corresponding to four different incident energies A, B, C and D , respectively. The first data point on each spectrum can be approximately unfolded by keeping only the first term and ignoring the two integrations in Eq. (IV.2); in the expressions for δ_t and δ_r , we take Δ equal to the vertical distance between the point (E_s, E_p) and the pion threshold when calculating $\ln(E_p/\Delta)$, but equal to the horizontal distance between the point (E_s, E_p) and the pion threshold when calculating $\ln(E_s/\Delta)$. The first point in each spectrum serve as the beginning for our entire subsequent unfolding program. We arrange the rest of the data points in all four spectra in sequence as an increasing function of the missing mass M_f . Then starting from the point with the lowest M_f , we proceed to unfold each data point individually by use of Eq.

(IV.2) together with an appropriate choice of Δ and an interpolation or extrapolation procedure to be discussed in the following. The quantity Δ in Eq. (IV.2) should not be confused with the interval between the data points. It is just an artificial device to handle the infrared divergence problem. In fact, one should always make sure that the final result is relatively insensitive to the choice of Δ , provided Δ is chosen small enough so that the variation of the cross section is negligible within this interval but large enough so that the neglect of region IV in Fig. 3 is justified. The error due to the neglect of region IV in Fig. 3 is expected to be roughly $\sim [(bT/2) \ln (E_s/\Delta)]^2$. Since the widths of the resonances are roughly ~ 100 MeV, Δ should be chosen to be less than 15 MeV in the resonance region. Assuming $b=4/3$, $T=0.03$ radiation lengths, and $E_s=10$ GeV, the error due to the neglect of region IV is roughly 0.16% of the cross section for $\Delta=15$ MeV and 0.22% for $\Delta=5$ MeV.

Due to limitations on available accelerator time, usually the cross section is measured at many values of the outgoing electron energy E'_p but only at a few values of the incident electron energy E_s . Therefore, interpolations and extrapolations of the cross sections are required when using Eq. (IV.2) to do the radiative corrections. For example let us consider the radiative corrections to the second data point (E_s, E_p) on spectrum A of Fig. 3. The integration with respect to dE'_p can be carried out readily over the spectrum *already unfolded*. However it requires some trick to perform the integration along the horizontal direction because there are no data points available. The important thing to notice is that the cross section for a fixed value of the missing mass M_f varies only monotonically as a function of incident energy at a fixed angle, whereas the cross section can vary rapidly with E_s along the constant E_p line. Hence it is most desirable to make the interpolations or extrapolations along the equimissing mass line rather than directly along the constant E_p line (see Fig. 4). Consider the integration with respect to dE'_s in Eq. (IV.2) for performing the radiative corrections to the second data point on the spectrum A . Suppose

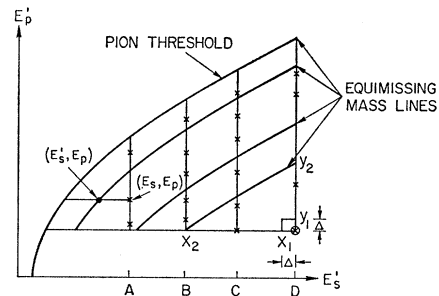


FIG. 4. Illustration of the unfolding procedure for each experimental data point. The cross represents a data point. We assume that there are four spectra corresponding to four incident energies A, B, C , and D available at one angle.

the nonradiative cross section $\sigma(E'_s, E_p)$ at point (E'_s, E_p) is required to perform the integration. This cross section can be extrapolated from the cross sections already unfolded in the following way: (1) Compute the missing mass M_f corresponding to the point (E'_s, E_p) where the cross section (nonradiative) is desired. (2) Use an appropriate interpolation or extrapolation formula to find the cross sections corresponding to this value of missing mass on spectra A, B, C , and D using only the already unfolded points in each spectrum. (3) Finally, extrapolate the cross sections obtained in step (2) to obtain the cross section at the desired point (E'_s, E_p) . This procedure works very well until we reach a very high missing mass value where the equimissing mass line passes through only spectra C and D (the equimissing mass line passes through only spectrum D at a still higher missing mass). Thus, when near the ends of spectra C and D , the extrapolation of the cross section can not be done using the procedure just described. We suggest a way to overcome this problem: (1) Usually when M_f is larger than 2 GeV, the resonances are small and the spectra change only monotonically as a function of M_f . Hence the spectra $A-C$ can be extrapolated downward somewhat without much loss in accuracy. This procedure will extend the range of the integrand in the dE'_s integration but will not cover the entire range required for the radiative corrections of the tail ends of spectra C and D . (2) With a reasonable choice of Δ , the first term in the right-hand side of Eq. (IV.2) contributes about 60%–70% and the two integrations in Eq. (IV.2) roughly contribute equally (15%–20% from each). Thus we divide the dE'_s integration into two parts, that which can be extrapolated or interpolated from the measured cross sections and that which can not, and replace this latter portion by the corresponding dE_p' integration. For example, in Fig. 4 we replace the integration from x_1 to x_2 by the integration from y_1 to y_2 . We have applied this procedure to the 3–3 resonance model mentioned previously and found that even if x_2 and y_2 are extended all the way to the pion threshold, the resulting error amounts to only a few percent of the cross section. This observation implies that even if there is only one spectrum measured at one angle, one can still do the radiative corrections approximately if willing to tolerate an error of $\lesssim 10\%$ in the cross section.

We have applied the unfolding procedure described above to the experimental results on the inelastic electron scattering data obtained by the electron scattering group at the Stanford Linear Accelerator Center.²⁶ The results are shown in Figs. 5(a)–5(f). Two curves are shown on each graph; they represent the raw experimental data and unfolded data, respectively. Figures 5(a)–5(d) represent four spectra measured at 7, 10, 13.5, and 16.02 GeV in incident energy and 6° , and they are unfolded simultaneously using the procedures described above. Figures 5(e) and 5(f) use the same

experimental data as shown in Figs. 5(a) and 5(d), but they were unfolded by assuming that the dE'_s integration is equal to the dE_p' integration in Eq. (IV.2). As is evident from our previous discussions, the more spectra one has at one angle, the more reliable is our procedure for the unfolding. Comparing Fig. 5(a) with 5(e), and Fig. 5(d) with 5(f), we observe that the results differ by at most 6% in cross sections. While an error of 6% may be tolerable for many purposes, it can become disastrous when one wants to separate the two form factors from data measured at two different angles.

C. Some Practical Considerations

The most important thing the experimentalists have to do is to plan the experiment from the beginning so that the radiative corrections can be carried out. We list several items in the following to assist such planning:

(1) The purpose of the experiment is to obtain $F(q^2, M_f^2)$ and $G(q^2, M_f^2)$ as functions of q^2 and M_f^2 . When the radiative process is ignored, q^2 and M_f^2 can be written as

$$-q^2 = 2sp = +4E_s E_p \sin^2 \frac{1}{2}\theta \quad (\text{IV.3})$$

and

$$M_f^2 = u^2 = M^2 + 2M(E_s - E_p) + q^2, \quad (\text{IV.4})$$

from which we have

$$E_s(q^2, M_f^2, \theta) = \frac{M_f^2 - M^2 - q^2}{4M} + \left(\frac{(M_f^2 - M^2 - q^2)^2}{16M^2} - \frac{q^2}{2(1 - \cos \theta)} \right)^{1/2}, \quad (\text{IV.5})$$

$$E_p(q^2, M_f^2, \theta) = -\frac{M_f^2 - M^2 - q^2}{4M} + \left(\frac{(M_f^2 - M^2 - q^2)^2}{16M^2} - \frac{q^2}{2(1 - \cos \theta)} \right)^{1/2}. \quad (\text{IV.6})$$

Hence for fixed q^2 and M_f^2 , we can choose two values of θ and obtain two sets of values for (E_s, E_p) from Eqs. (IV.5) and (IV.6). Let us denote them by $[E_s(\theta_1), E_p(\theta_1), q^2, M_f^2]$ and $[E_s(\theta_2), E_p(\theta_2), q^2, M_f^2]$, respectively. The form factors $F(q^2, M_f^2)$ and $G(q^2, M_f^2)$ can be separated out from the knowledge of the nonradiative cross sections at these two sets of kinematical conditions by solving two simultaneous linear equations using Eq. (B.1):

$$F(q^2, M_f^2) + (2/M^2) \tan^2(\theta_1/2) G(q^2, M_f^2) = X[E_s(\theta_1), E_p(\theta_1), q^2, M_f^2], \quad (\text{IV.7})$$

$$F(q^2, M_f^2) + (2/M^2) \tan^2(\theta_2/2) G(q^2, M_f^2) = X[E_s(\theta_2), E_p(\theta_2), q^2, M_f^2], \quad (\text{IV.8})$$

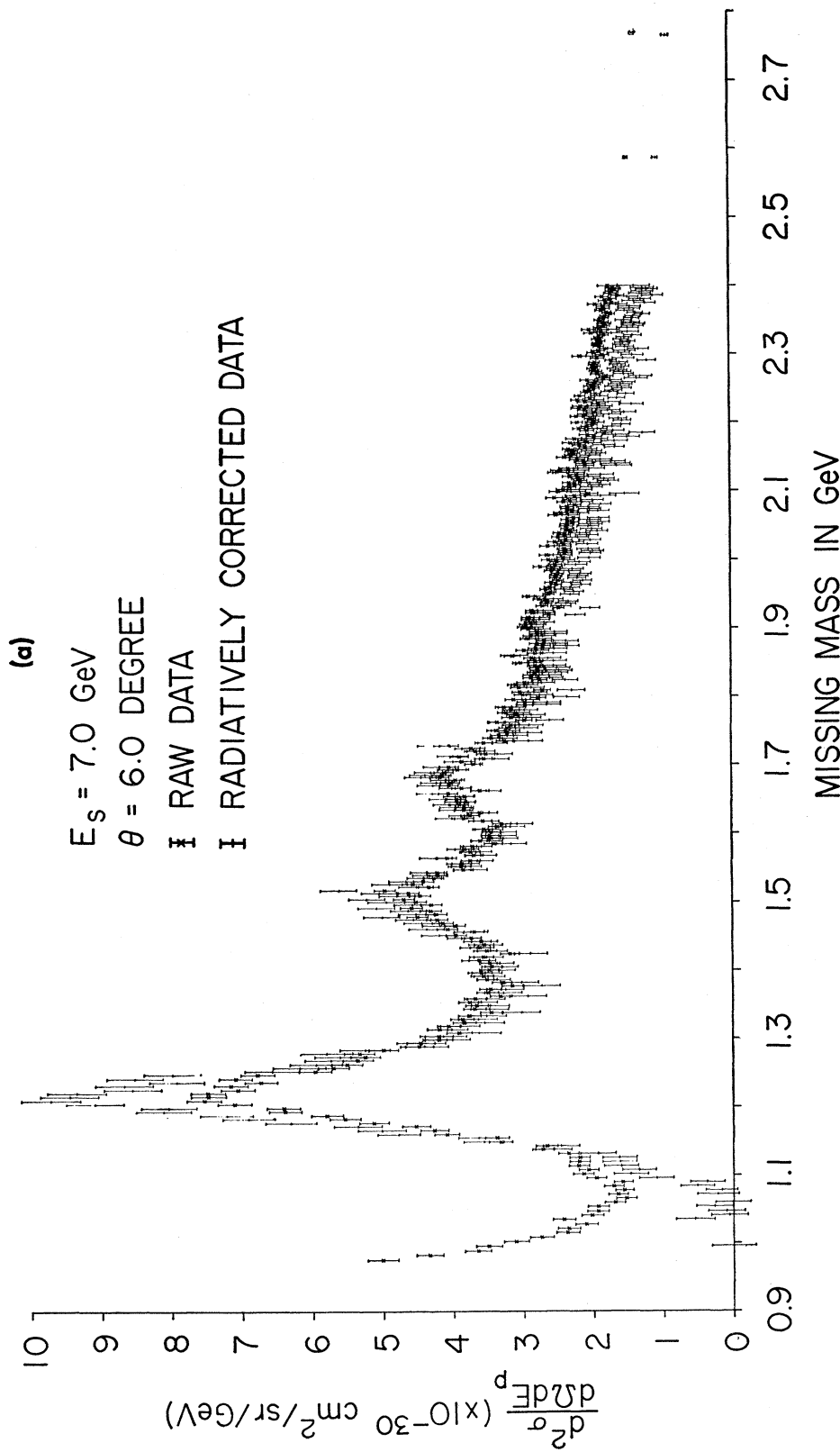


FIG. 5. Examples of unfolding the actual experimental $e\bar{\nu}$ inelastic spectra. The data are the preliminary results of the SLAC electron scattering group reported in Ref. 26. All data are measured at 6° with incident electron energy values shown in the figure. Results of the radiative corrections shown in (a)-(d) are obtained by the simultaneous unfolding procedure described in the text. In (e) and (f), the radiative corrections are done by the approximation that the two integrals in Eq. (VI.2) are equal to each other. The thicknesses of the radiator before the target, the liquid-hydrogen target, and the radiator after the target are 0.00172, 0.00862, and 0.00691 radiation lengths, respectively. It should be noted that after the subtraction of the elastic tail, the cross section between the elastic peak and the pion threshold becomes zero using the method described in Sec. III.A.

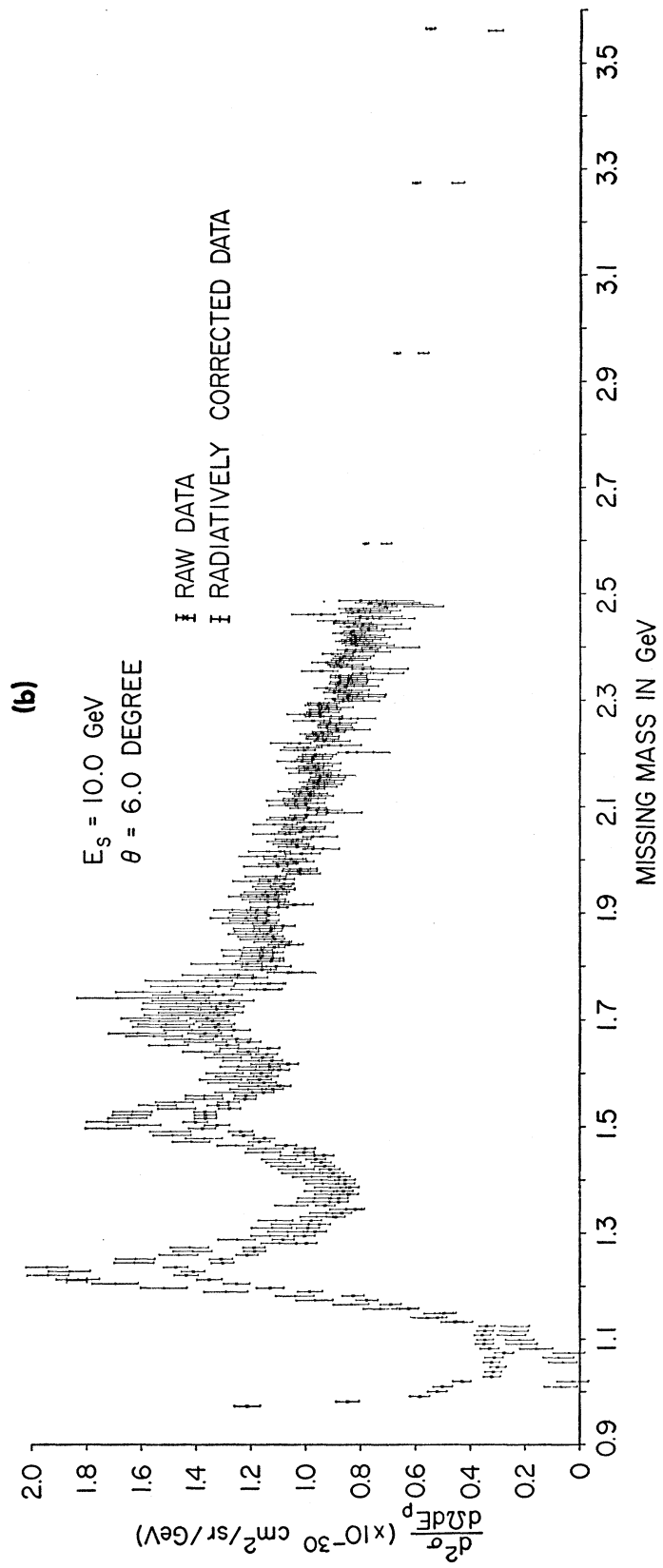


FIG. 5 (Continued)

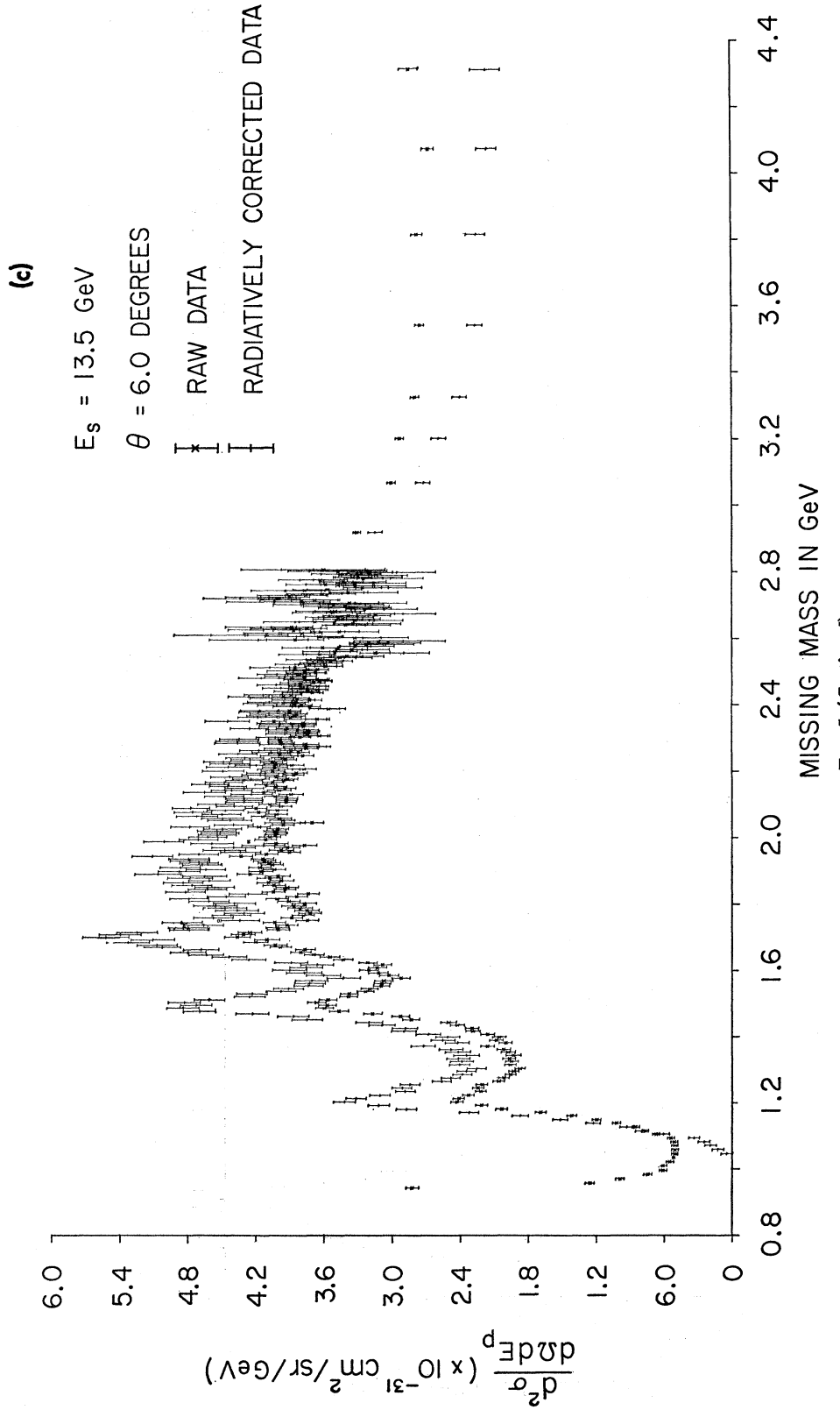


FIG. 5 (Continued)

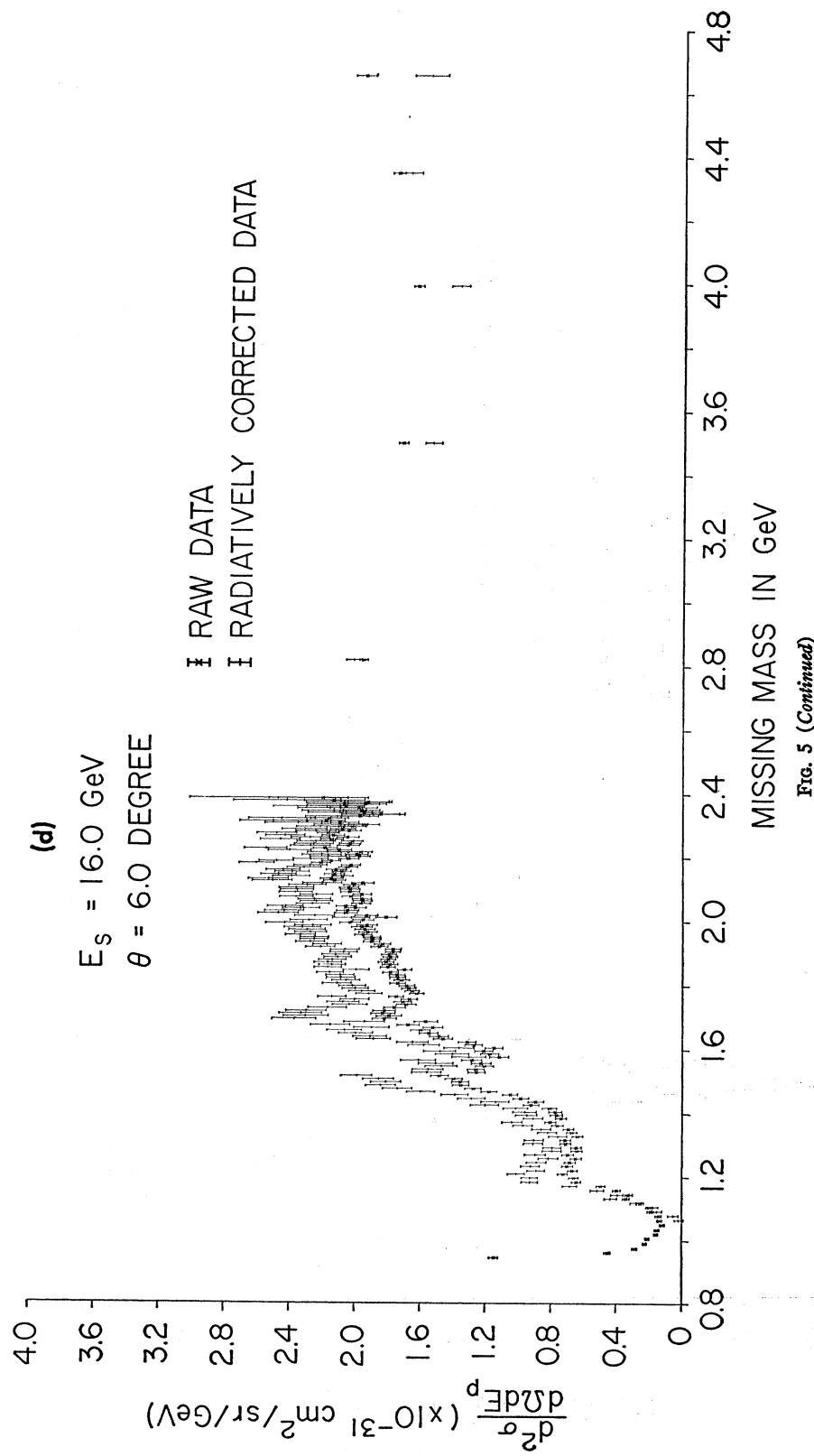


FIG. 5 (Continued)

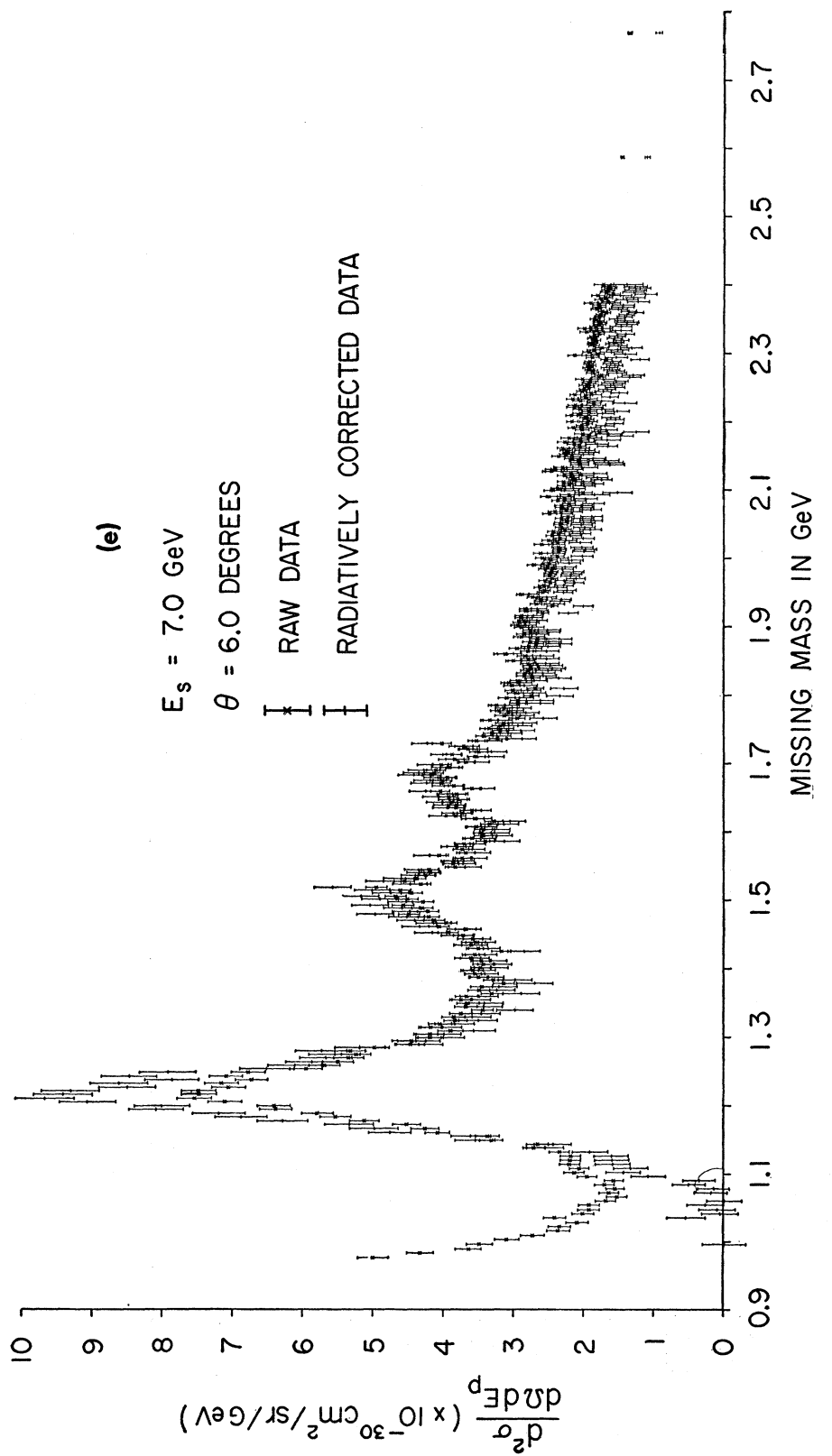


FIG. 5 (Continued)

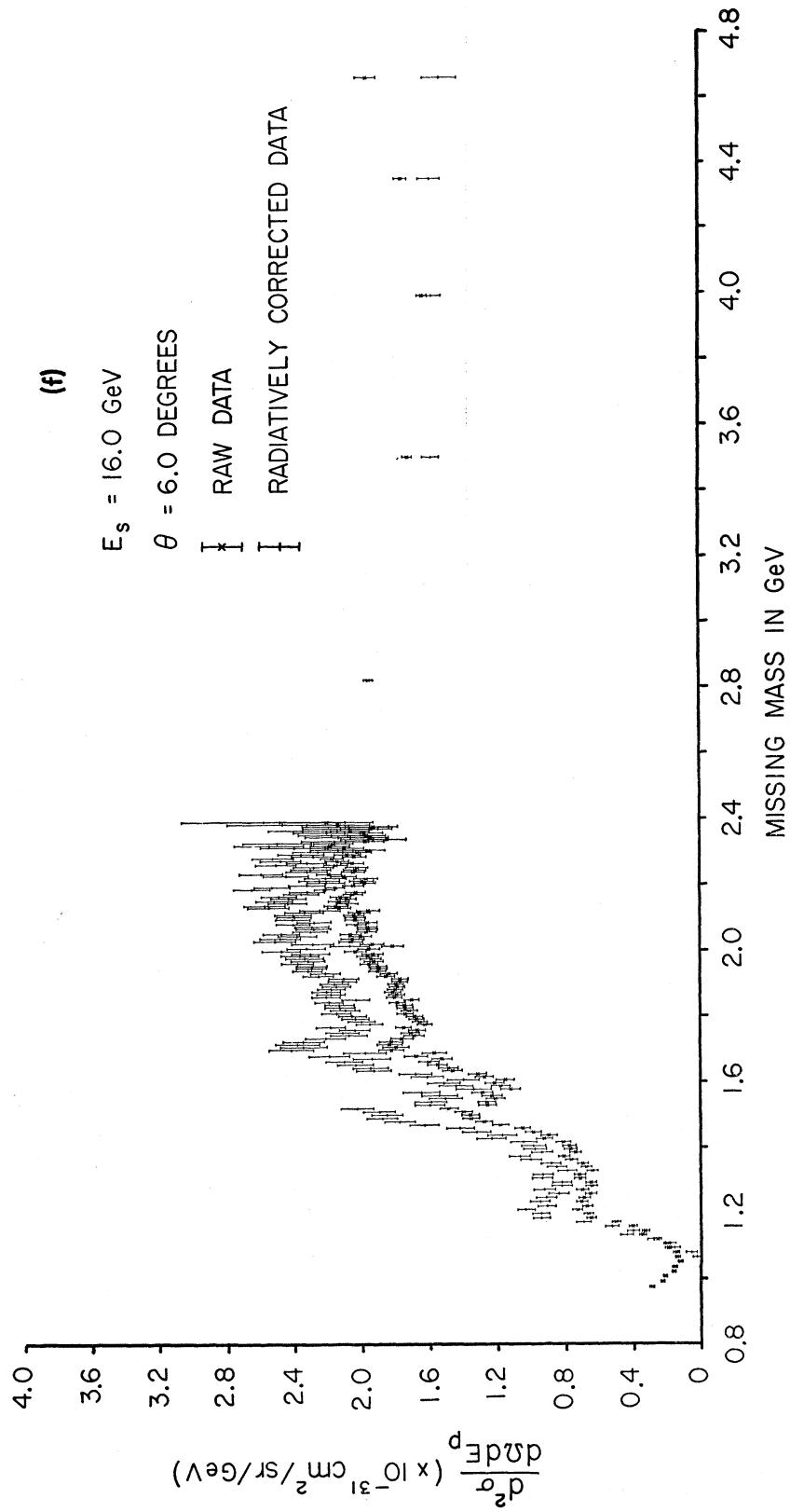


FIG. 5 (*Conclusion*)

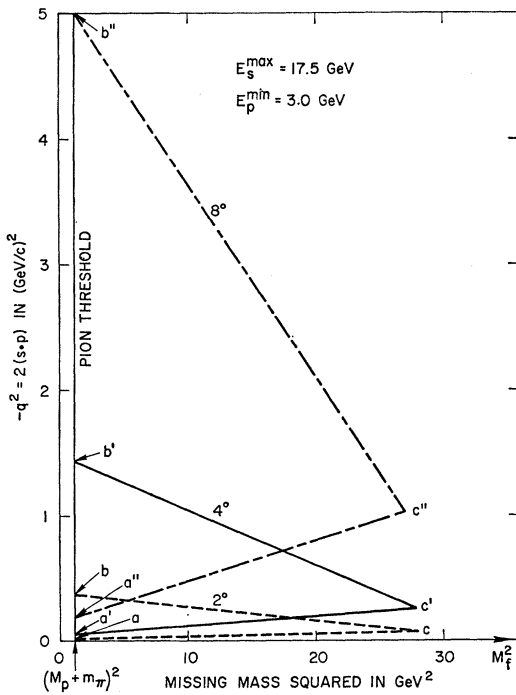


FIG. 6. Examples of overlap in the $(2s\bar{p}, M_f^2)$ plane for three values of $[E_s^{\max}(\theta), E_p^{\min}(\theta)]$ represented by point c' in Fig. 3 at three angles θ_1 , θ_2 , and θ_3 . The separation of form factors is possible only when two triangles overlap.

where X is the cross section divided by the kinematical factor in front of the bracket in Eq. (B.1).

(2) In order to do radiative corrections, one needs to take data at many different incident energies at *one angle*. The values of the cross sections at different angles are *not required* to perform the radiative corrections. *The number of points measured inside the shaded area abc in Fig. 3 must be dense enough so that interpolation between points can be carried out.* In the shaded area of Fig. 3, the lines parallel to ab represent the "equimissing mass lines"; for example, line ab represents $u^2 = (M_p + m_\pi)^2$, the missing mass corresponding to the pion threshold, and the next line represents, say, $u^2 = (1236 \text{ MeV})^2$, etc. The point c has the highest missing mass. The lines intersecting the "equimissing mass lines" represent the "equimomentum transfer lines"; $2s\bar{p}$ is minimum at point "a," whereas it is maximum at point "b." Let us suppose an experimentalist wants to measure cross sections at an angle θ within the range of E_s' and E_p' shown by the shaded area of Fig. 3. The kinematic region indicated by the shaded area is uniquely determined by the angle θ and the position of point c , which we will denote by $c(E_s^{\max}, E_p^{\min}, \theta)$. For any given $c(E_s^{\max}, E_p^{\min}, \theta)$ we can map the shaded area of Fig. 3 onto an area in the $(M_f^2, 2s\bar{p})$ plane. This area is bounded by the following inequalities:

$$(M + m_\pi)^2 \leq M_f^2 \leq M^2 + 2M(E_s^{\max} - E_p^{\min}) - 2E_s^{\max}E_p^{\min}(1 - \cos \theta) \quad (\text{IV.9})$$

and

$$\begin{aligned} 2E_p^{\min}(1 - \cos \theta) \frac{M_f^2 - M^2 + 2ME_p^{\min}}{2M - 2E_p^{\min}(1 - \cos \theta)} &\leq 2s\bar{p} \\ &\leq 2E_s^{\max}(1 - \cos \theta) \frac{M^2 - M_f^2 + 2ME_s^{\max}}{2M + 2E_s^{\max}(1 - \cos \theta)}. \quad (\text{IV.10}) \end{aligned}$$

Equation (IV.9) gives the range of the missing mass covered by the experiment and Eq. (IV.10) gives the range of momentum transfer for each value of M_f^2 . The area bounded by Eqs. (IV.9) and (IV.10) is a triangle in the $(M_f^2, 2s\bar{p})$ plane. Hence each shaded area in Fig. 3 can be mapped onto a triangle in the $(M_f^2, 2s\bar{p})$ plane. In order to determine the form factors from Eqs. (IV.7) and (IV.8), one has to measure another set of cross sections at a different angle. The latter set of data must also consist of points which are represented by a shaded area shown in Fig. 3 in order to do radiative corrections. Let us again represent this area by the position of point c' in Fig. 3 and denote it by $c'(E_s^{\max'}, E_p^{\min'}, \theta')$. This new kinematical region can again be mapped onto a triangle in the $(M_f^2, 2s\bar{p})$ plane. It is obvious that only in the regions where two triangles overlap can one determine the form factors $F(q^2, M_f^2)$ and $G(q^2, M_f^2)$. In Fig. 6 we have plotted three triangles corresponding to three sets of c' 's: $c(17.5 \text{ GeV}, 3 \text{ GeV}, 2^\circ)$, $c'(17.5 \text{ GeV}, 3 \text{ GeV}, 4^\circ)$ and $c''(17.5 \text{ GeV}, 3 \text{ GeV}, 8^\circ)$. The points a , b , and c in Fig. 3 have the same kinematical significance as points a , b and c in Fig. 6. From the overlapping region of the two triangles $a'b'c'$ and $a''b''c''$ we see, for example, that the separation of form factors for the 3-3 resonances at $M_f^2 = (1.236)^2 = 1.53 \text{ GeV}^2$ is possible in the range $0.2 \text{ GeV}^2 < 2s\bar{p} < 1.41 \text{ GeV}^2$. The measurements are assumed to be made at 4° and 8° , with incident energies of up to 17.5 GeV . All the spectra are assumed to be measured down to 3 GeV .

D. Final Check of Reliability of Approximate Formula

After the inelastic form factors have been obtained, we can use them to calculate the radiative tail using the exact formula, Eq. (B.6). The results can then be utilized to check the reliability of the original approximations made to obtain these form factors.

V. DISCUSSIONS AND SUMMARY

In Fig. 7, we plotted five curves:

(1) Elastic radiative tail from $e\bar{p}$ scattering using our exact formula, Eq. (B.5) (see Column 3 of Table III).

(2) A curve similar to the above but using the method of equivalent radiators, using Eqs. (III.15), (C.11), (B.3), (III.2), (III.3) (see Column 7 of Table III).

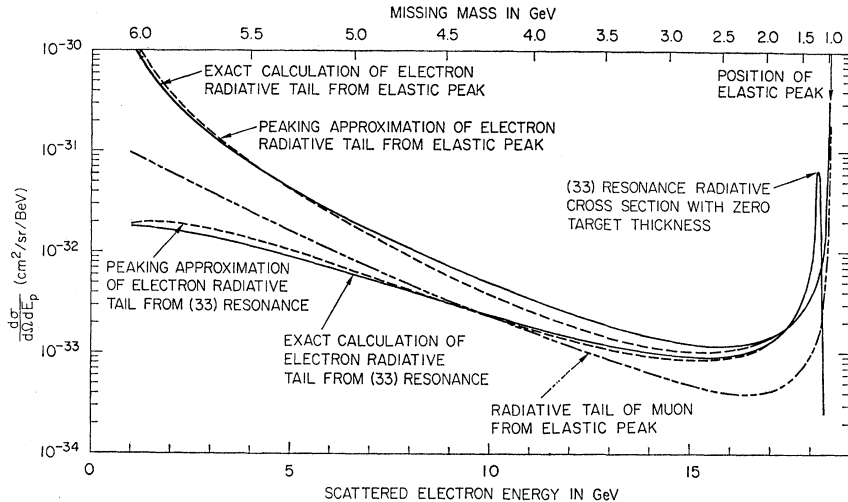


FIG. 7. Examples of radiative tails from $e\bar{p}$ and $\mu\bar{p}$ elastic scattering. Also shown is the radiative tail from 3-3 resonance. The incident energy is 20 GeV, and the scattering angle is 5° .

(3) The 3-3 resonance with radiative corrections [see Fig. 2(a)] and its radiative tail using the method of equivalent radiators (see Column 5 of Table IV).

(4) The radiative tail from the 3-3 resonance using our exact formula, Eq. (B.5), with the zero-width approximation for the 3-3 peak [Eq. (III.11) and see Column 3 of Table IV].

(5) The radiative tail from $\mu\bar{p}$ elastic scattering using Eq. (B.5).

All five curves are calculated for an incident energy $E_e = 20$ GeV, scattering angle $\theta = 5^\circ$, and with the straggling effect in the target ignored. These curves illustrate the over-all behavior of the radiative tails from elastic $e\bar{p}$ and $\mu\bar{p}$ scatterings and $e+p \rightarrow e+N^*$. They also illustrate the reliability of the approximation formula used. We should notice that at this incident energy and scattering angle, the elastic cross section and the 3-3 resonant cross section are comparable in magnitude (2.2×10^{-32} and 1.61×10^{-32} cm^2/sr , respectively). However, the radiative tail from the elastic peak is much more prominent than that from the 3-3 resonance, except in the neighborhood of the 3-3 peak. The order of magnitude of the ratio of the $\mu\bar{p}$ to $e\bar{p}$ radiative tail is roughly given by $[\ln(2sp/m_\mu^2) - 1] \times [\ln(2sp/m_e^2) - 1]^{-1}$.

We have investigated and improved the reliability of many formulas used in calculating radiative corrections to elastic and inelastic electron scatterings when only the scattered electrons are detected. The uncertainties still left are the contributions from (a) multiple photon exchange between the hadron current and the electron current and (b) the effect of the real photon emissions from the hadronic system. These two effects have to be treated together in order to achieve cancellation of the infrared divergences. Except in the infrared limit, both of these effects depend upon the detailed structure of the strong interactions, which are hard to calculate. In the formula for the radiative

corrections to the *elastic peak*, these two effects have been calculated in the infrared limit and are given by the terms proportional to Z^1 and Z^2 in Table I. The terms proportional to Z^1 represent two-photon exchange contributions and the interference terms between the electron-bremsstrahlung and the hadron-bremsstrahlung diagrams. The terms proportional to Z^2 come from the square of the hadron-bremsstrahlung matrix elements. It is reasonable to assume that the ratios of Z^1 terms to Z^0 terms, and of Z^2 terms to Z^0 terms, from the *elastic* radiative corrections roughly give the order of magnitude of the corresponding contributions from the *inelastic* excitation of the hadronic system. When positrons are used, Z^1 terms change sign. We notice also from Table I that Z^1 and Z^2 terms are comparable in magnitude. Hence, the most practical way to determine the significance of the above-mentioned two effects is to make some spot comparisons of the experimental *inelastic* spectra for positron scattering with those for electron scattering. If the difference is small, these two effects are probably negligible; if not, then one should start worrying about them.

In summary let us sketch an ideal procedure for doing radiative corrections:

(1) Perform $e^+\bar{p}$ and $e^-\bar{p}$ elastic scatterings at various energies and angles. Compare the experimental results with formulas given by T and MY (see Sec. II) and select the version which gives a better agreement with the experimental results. Perform the radiative corrections using Eq. (II.9) and obtain elastic form factors $G_e(q^2)$ and $G_m(q^2)$.

(2) Use Figs. 3 and 4 to determine the desirable ranges of momentum transfer q^2 and missing mass M_f^2 to be investigated by the experiment. Take data at two angles; the data at each angle must consist of many incident energies so that interpolation between points inside the shaded area shown in Fig. 3 is possible.

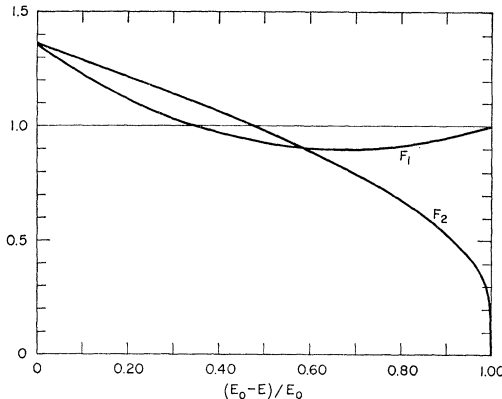


FIG. 8. Comparison of Eq. (A.6) with Eq. (A.9) for $Z=1$. The curves plotted represent $(d\sigma/dE)X_0NA^{-1}(E_0-E)$. F_1 corresponds to Eq. (A.9) and F_2 corresponds to Eq. (A.6).

(3) Calculate the radiative tail from the elastic peak using Eq. (III.1) and subtract its contribution from each inelastic spectrum. It should be emphasized that our exact formula, Eq. (B.5), must be used for this purpose.

(4) Perfect the procedure for doing radiative corrections to inelastic spectra by carrying out the exercise mentioned in Sec. IV. First: starting with a given *nonradiative* 3-3 resonance cross section, calculate the *radiative* cross section using Eq. (IV.1). Then perform a reverse calculation using Eq. (IV.2) to see if one can obtain the original nonradiative cross section. This exercise not only enables one to perfect the procedure for performing the radiative corrections before the data become available, but also can tell one how many data points need to be taken within the shaded area of Fig. 3 in order to carry out the radiative correction satisfactorily.

(5) Apply the radiative corrections to inelastic spectra using the procedure obtained in Sec. IV. Obtain inelastic form factors $F(q^2, M_f^2)$ and $G(q^2, M_f^2)$ using Eqs. (IV.7) and (IV.8).

(6) Take the data on e^+p *inelastic* scattering at a few points and compare the results with those on e^-p scattering. The difference between the two cross sections represents the uncertainty due to multiple photon exchange and the bremsstrahlung by the hadronic system.

ACKNOWLEDGMENTS

The authors would like to thank A. J. Dufner and D. Tompkins for their careful reading of the manuscript and useful suggestions.

APPENDIX A: STRAGGLING EFFECT

As mentioned in the introduction, the straggling effect of the electron in the target is very similar to the radiative corrections, and the magnitude of the two effects are often comparable in most of the experimen-

tal conditions. Hence the effect of straggling must be treated with as much care as the radiative corrections. In the literature, the straggling formula given by Bethe and Heitler,²⁷

$$I_e(E_0, E, t) = E_0^{-1} \frac{[\ln(E_0/E)]^{(t/\ln 2)-1}}{\Gamma(t/\ln 2)}, \quad (\text{A.1})$$

has often been used to calculate the straggling effects. The function $I_e(E_0, E, t)dE$ represents the probability of finding an electron in the energy interval dE after an electron, initially with energy E_0 , travelled a distance t (in units of radiation length) in the target. Equation (A.1) is adequate for an order-of-magnitude estimate, but is not accurate enough when an accuracy of better than 20% (in evaluating the straggling effect) is required. In most of the experiments, the target thickness is less than 0.05 radiation lengths; and as will be shown later in actual applications, the straggling effect can be approximated by assuming that the target is divided in half, and that one of the halves is placed before the scattering and one after. Hence t in Eq. (A.1) is less than 0.025 radiation lengths and $\Gamma(x)$ for small x can always be replaced by x^{-1} . We are also interested in E_0 and E , both larger than 1 GeV; hence the only electron energy attenuation of importance is that due to bremsstrahlung (we can ignore ionization). For the same reason we can use the bremsstrahlung cross section with complete screening except near the bremsstrahlung tip ($k \sim E_0$ or $E \rightarrow 0$). The deviation from the complete screening formula occurs only when the minimum momentum transfer to the target is larger than, or comparable to, the inverse of the atomic radius; hence, the complete screening formula is correct as long as we disregard the region

$$\frac{E}{E_0} = 1 - \left(\frac{k}{E_0}\right) < \frac{137m}{2Z^{1/3}E_0 + 137m} \simeq 0.03$$

for $Z=1, E_0=1$ BeV. (A.2)

Under the conditions specified above, we propose that Eq. (A.1) should be replaced by

$$I_e(E_0, E, t) = bt(E_0-E)^{-1} \left[\frac{E}{E_0} + \frac{3}{4} \left(\frac{E_0-E}{E_0} \right)^2 \right] \left[\ln \frac{E_0}{E} \right]^{bt}, \quad (\text{A.3})$$

where

$$b = \frac{4}{3} \left\{ 1 + \frac{1}{9} [(Z+1)/(Z+\xi)] [\ln(183Z^{-1/3})]^{-1} \right\} \quad (\text{A.4})$$

and

$$\xi = \ln(1440Z^{-2/3})/\ln(183Z^{-1/3}). \quad (\text{A.5})$$

We believe Eq. (A.3) is accurate to within 1% in the range $0.5E_0 < E < E_0$ and within 2% in the range $0.05E_0 < E < 0.5E_0$ by the following reasoning:

(1) It was first shown by Bethe and Heitler²⁷⁻²⁹ that if the cross section for the bremsstrahlung were given by

$$d\sigma/dE = (bA/X_0N)[E_0 \ln(E_0/E)]^{-1}, \quad (\text{A.6})$$

then $I_e(E_0, E, t)$ would be given rigorously by

$$I_e(E_0, E, t) = E_0^{-1} \frac{[\ln(E_0/E)]^{bt-1}}{\Gamma(bt)}, \quad (\text{A.7})$$

where A is atomic weight, N is Avogadro's number, and X_0 is the unit radiation length in grams per square centimeter. The actual form of the cross section is quite different from Eq. (A.6), especially when $E < 0.35E_0$, as can be seen from Fig. 8.

(2) From Eq. (A.6) and Eq. (A.7) we notice that when bt is small, Eq. (A.7) can be written as

$$I_e(E_0, E, t) = \left(\frac{N}{A} X_0 t \frac{d\sigma}{dE} \right) \left(\ln \frac{E_0}{E} \right)^{bt}. \quad (\text{A.8})$$

If the electron encounters the atoms in the target at most once, then one would have obtained only the first factor on the right-hand side of Eq. (A.8). Hence the term $(\ln E_0/E)^{bt}$ can be regarded as a correction due to the multiple encounters. Now all we have to do is to insert a correct expression for $d\sigma/dE$ into (A.8), instead of using Eq. (A.6), and show that the correction factor $(\ln E_0/E)^{bt}$ is relatively insensitive to the fact that Eq. (A.6) is a bad approximation when $E < 0.35E_0$.

(3) The correct expression for $d\sigma/dE$ corresponding to one-photon emission and complete screening is given by³⁰

$$\frac{d\sigma}{dE} = X_0^{-1} \frac{A}{N} \frac{4}{3} (E_0 - E)^{-1} \left[\frac{E}{E_0} + \frac{3}{4} \left(\frac{E_0 - E}{E_0} \right)^2 \right] \left(1 + \frac{E}{9E_0} \frac{Z+1}{Z+\xi} [\ln(183Z^{-1/3})]^{-1} \right), \quad (\text{A.9})$$

where X_0 is the unit radiation length given by Bethe and Ashkin²⁹

$$1/X_0 = (4N/A) \alpha r_0^2 Z(Z+\xi) \ln(183Z^{-1/3}). \quad (\text{A.10})$$

Comparison of Eqs. (A.9) and (A.6) shows if b is chosen to be that given by Eq. (A.4), then the two expressions agree completely in the infrared limit ($E \rightarrow E_0$), and Eq. (A.9) is only 1% less than Eq. (A.6) when $E = 0.98E_0$. In Fig. 6 we compare numerical values of Eq. (A.6) and Eq. (A.9). It is seen that Eq. (A.6) and Eq. (A.9) agree numerically within

10% up to $E = 0.35E_0$, but differ drastically for $E < 0.35E_0$.

(4) The shape of the bremsstrahlung spectrum at a high photon energy k ($k = E_0 - E$) should not affect the correction factor $(\ln E_0/E)^{bt}$ for high E , because if a hard photon is emitted, E will no longer be high. Since Eq. (A.9) agrees with Eq. (A.6) to within 10% in the range $0.35E_0 < E < E_0$, the correction factor $(\ln E_0/E)^{bt}$ must be substantially correct in this energy range. This factor is less than one when $E > 0.37E_0$ and greater than one when $E < 0.37E_0$. Hence the over-all effect of this factor is to deplete the number of high-energy electrons and to increase the number of low-energy electrons, a very intuitively plausible effect. Since the number of electrons removed from the high-energy side of the spectrum is roughly the same in two cases, we expect the number of electrons moved into the low-energy side must be roughly the same in two cases because of the conservation of leptons. In the region $E < 0.35E_0$, the spectrum given by Eq. (A.6) is less than that given by Eq. (A.9); hence we expect the correction factor for Eq. (A.9) must be less than that for Eq. (A.6). But the correction factor for Eq. (A.6) is only slightly larger than unity in this region. For example, $(\ln E_0/E)^{4/3t} \approx 1.03$ for $E = 0.05E_0$ and $t = 0.02$. Even if this factor is totally wrong, the error is at most 3% at this energy. In reality the error is probably less than 2%. We will not consider the region where $E < 0.05E_0$ because the complete screening formula is unreliable near the bremsstrahlung tip.

From Eq. (A.3) the fraction of electrons, initially with energy E_0 , which have an energy in the range $E_0 - \Delta \leq E \leq E_0$ after passing through a target of thickness t is given by

$$\begin{aligned} \int_{E_0-\Delta}^{E_0} I_e(E_0, E, t) dE &= \left(\frac{\Delta}{E_0} \right)^{bt} \quad \text{for } \left(\frac{\Delta}{E_0} \right) \ll 1 \\ &= \exp[-bt \ln(E_0/\Delta)] \\ &= 1 - bt \ln(E_0/\Delta) + \dots \end{aligned} \quad (\text{A.11})$$

Suppose an electron suffers a single large angle ($\theta \gg m/E_0$) scattering in a target of thickness T with a cross section $(d\sigma/d\Omega dE_p')(E_s', E_p', \theta) = \sigma(E_s', E_p')$; then because of straggling, the measured cross section would be given by

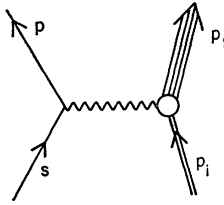
$$\begin{aligned} \sigma_t(E_s, E_p, T) &= d\sigma_t/d\Omega dE(E_s, E_p, T) \\ &= \int_0^T \frac{dt}{T} \int_{E_{s \min}(E_p)}^{E_s} dE_s' \int_{E_p}^{E_{p \max}(E_s')} dE_p' I_e(E_s, E_s', t) \sigma(E_s', E_p') I_e(E_p', E_p, T-t), \end{aligned} \quad (\text{A.12})$$

where $E_{s \min}(E_p)$ is the minimum value of E_s' allowed by the kinematics of $\sigma(E_s', E_p')$ when $E_p' = E_p$ and $E_{p \max}(E_s')$ is the maximum value of E_p' for a given E_s' . We shall use Eq. (A.12) to calculate three things.

(a) Effect of straggling on the elastic peak radiative

corrections: For elastic scattering we have

$$\begin{aligned} \sigma(E_s', E_p') &= d\sigma/d\Omega dE_p'(E_s', E_p') \\ &= [d\sigma_0(E_s')/d\Omega] \eta \delta(E_s' - E_p' - E_s'E_p'M^{-1}(1 - \cos \theta)), \end{aligned} \quad (\text{A.13})$$

FIG. 9. Feynman diagram for non-radiative $e\bar{p}$ inelastic scattering.

where

$$\eta = 1 + E_s' M^{-1} (1 - \cos \theta) \approx 1 + E_s M^{-1} (1 - \cos \theta). \quad (\text{A.14})$$

Substituting (A.13) into (A.12) and integrating the result with respect to E_p from $E_{p \max} - \Delta E$ to $E_{p \max}$, we obtain

$$\int_{E_{p \max} - \Delta E}^{E_{p \max}} \sigma_t(E_s, E_p, T) dE_p = \left(\frac{\Delta E}{E_{p \max}} \right)^{bT/2} \left(\frac{\Delta E \eta^2}{E_s} \right)^{bT/2} \times \frac{d\sigma_0}{d\Omega}(E_s), \quad (\text{A.15})$$

where

$$E_{p \max} = E_s / [1 + E_s M^{-1} (1 - \cos \theta)] = E_s \eta^{-1}.$$

Equation (A.15) can be derived under the assumptions $\Delta E / E_{p \max} \ll 1$ and $bT \ll 1$. The detail is straightforward but messy. Equation (A.15) is used in Eq. (II.9).

(b) Effect of straggling on the radiative tail of the elastic peak: This is similar to (a) except now we are interested in the value of E_p not very close to $E_{p \max}$. In this case we have from Eq. (A.12)

$$\begin{aligned} \frac{d\sigma_{0,t}}{d\Omega dE_p}(E_s, E_p, T) &= I_e(E_s, E_p \eta_1, \frac{1}{2}T) \eta_1^2 \frac{d\sigma_0}{d\Omega}(E_p \eta_1) \\ &+ I_e(E_s \eta_2^{-1}, E_p, \frac{1}{2}T) \frac{d\sigma_0}{d\Omega}(E_s), \end{aligned} \quad (\text{A.16})$$

where

$$\eta_1 = [1 - E_p M^{-1} (1 - \cos \theta)]^{-1},$$

$$\eta_2 = 1 + E_s M^{-1} (1 - \cos \theta),$$

and I_e is given by Eq. (A.3).

(c) Effect of straggling on the radiative correction to the continuum state: Let us assume that the elastic radiative tail has been subtracted from the inelastic spectrum already. Then the limits of integration $E_{s \min}(E_p)$ and $E_{p \max}(E_s)$ in Eq. (A.12) are given by the kinematics of the electro-pion production at the threshold, namely

$$(M + m_\pi)^2 = M^2 + 2M(E_s' - E_p') - 2E_s'E_p'(1 - \cos \theta). \quad (\text{A.17})$$

Hence

$$\begin{aligned} E_{s \min}(E_p) &= (m_\pi^2 + 2Mm_\pi + 2ME_p) / [2M - 2E_p(1 - \cos \theta)] \\ &\quad (\text{A.18}) \end{aligned}$$

and

$$\begin{aligned} E_{p \max}(E_s') &= (2ME_s' - 2Mm_\pi - m_\pi^2) / [2M + 2E_s'(1 - \cos \theta)] \\ &\quad (\text{A.19}) \end{aligned}$$

The region of integration in Eq. (A.12) is shown by the shaded area in Fig. 3. In order to avoid the singularities of the integrand at $E_s = E_s'$ and $E_p = E_p'$, it is a good idea to separate the region of integration into four regions as shown in Fig. 3. The cross section $\sigma(E_s', E_p')$ is smooth compared with $I_e(E_s, E_s', t)$ and $I_e(E_p', E_p, T-t)$. For simplicity let us suppose Δ is chosen such that $bT \ln(E_s/\Delta) < 0.2$ and $bT \ln(E_p/\Delta) < 0.2$; then from Eq. (A.11) we expect that region I would contribute more than 64%, region II more than 16%, region III more than 16%, and region IV less than 4% to the integration. If we ignore region IV, we obtain [using Eq. (A.11)]

$$\begin{aligned} \frac{d\sigma}{dE_p d\Omega}(E_s, E_p, T) &= \int_0^T \frac{dt}{T} \left[\left(\frac{\Delta}{E_s} \right)^{bt} \left(\frac{\Delta}{E_p} \right)^{b(T-t)} \sigma(E_s, E_p) \right. \\ &+ \left(\frac{\Delta}{E_p} \right)^{b(T-t)} \int_{E_{s \min}(E_p)}^{E_s - \Delta} I_e(E_s, E_s', t) \sigma(E_s', E_p) dE_s' \\ &+ \left. \left(\frac{\Delta}{E_s} \right)^{bt} \int_{E_p + \Delta}^{E_{p \max}(E_s)} I_e(E_p', E_p, T-t) \sigma(E_s, E_p') dE_p' \right] \end{aligned} \quad (\text{A.20})$$

$$\begin{aligned} &\simeq \left(1 - \frac{1}{2}(bT) \ln \frac{E_s}{\Delta} - \frac{1}{2}(bT) \ln \frac{E_p}{\Delta} \right) \sigma(E_s, E_p) \\ &+ \int_{E_{s \min}(E_p)}^{E_s - \Delta} I_e(E_s, E_s', \frac{1}{2}T) \sigma(E_s', E_p) dE_s' \\ &+ \int_{E_p + \Delta}^{E_{p \max}(E_s)} I_e(E_p', E_p, \frac{1}{2}T) \sigma(E_s, E_p') dE_p'. \end{aligned} \quad (\text{A.21})$$

We have assumed that the variation of the cross section is negligible when E_s and E_p are changed by a small amount Δ . Since the widths of the resonances are typically 100~150 MeV, Δ should be taken less than ~ 15 MeV. When $E_s = 20$ GeV and $bT/2 = 0.03$ radiation lengths, we have $\frac{1}{2}bT \ln(E_s/\Delta) > 0.2$. Hence neglect of region IV and terms proportional to $[\frac{1}{2}bT \ln(E_s/\Delta)]$ causes an error of $\sim 4\%$. This is somewhat undesirable. We remedy this defect using the following criteria:

- (1) We insist on ignoring region IV in Fig. 3 to save computation time.

(2) The expression must be accurate up to terms of the order of $[\frac{1}{2}bT \ln(E_{s,t}/\Delta)]^2$ compared with the correct expression when the cross section is constant.

(3) The expression must be relatively insensitive to the choice of Δ when the cross section is constant.

Using these criteria, we propose the following expression as a substitute for Eq. (A.21):

$$\begin{aligned} \frac{d\sigma_t}{dE_p d\Omega}(E_s, E_p, T) = & \exp(\delta_s + \delta_p) \sigma(E_s, E_p) \\ & + \exp(\frac{1}{2}\delta_p) \int_{E_{s,\min}(E_p)}^{E_s - \Delta} I_e(E_s, E_s', \frac{1}{2}T) \sigma(E_s', E_p) dE_s' \\ & + \exp(\frac{1}{2}\delta_s) \int_{E_p + \Delta}^{E_p, \max(E_s)} I_e(E_p', E_p, \frac{1}{2}T) \sigma(E_s, E_p') dE_p', \end{aligned} \quad (\text{A.22})$$

where

$$\delta_{s,p} = -\frac{1}{2}bT \ln(E_{s,p}/\Delta).$$

When the cross section is constant we expect that the right-hand side must be equal to the left-hand side of Eq. (A.22). Expanding the right-hand side of (A.22) in power series of $\delta_{s,p}$, we see that the left-hand side is equal to the right hand side up to terms of order $\delta_{s,p}^2$. Hence the criterion (2) is satisfied. Again if we assume that the cross section is constant and differentiate the right-hand side of (A.22) with respect to Δ , we see that the resultant expression is equal to zero up to the terms of the order $\delta_{s,p}^2$. Hence the criterion (3) is satisfied. What we have accomplished is essentially the nearly complete elimination of the error introduced by neglecting region IV. Furthermore, we have made our expression relatively insensitive to the choice of Δ [see discussions after Eq. (IV.1) in Sec. IV]. We shall refer to the approximation in which region IV in Fig. 3 is neglected as the strip approximation.

APPENDIX B: EXACT CALCULATION OF RADIATIVE TAILS

It was shown by Tsai¹³ that the radiative tails from an arbitrary unpolarized target system and arbitrary hadronic final state can be calculated exactly in the lowest order of α if (1) the one-photon exchange mechanism is assumed, (2) the interference terms between the electron bremsstrahlung and the hadron bremsstrahlung are ignored, and (3) only the scattered electrons are detected.

This can be done because in the one-photon exchange model, the nonradiative cross section (see Fig. 9) depends upon two form factors, and the radiative cross section (see Fig. 10) also depends upon the same two form factors. We shall reproduce here the formulas given in Ref. 13 for completeness. Let us normalize these form factors by the nonradiative cross section

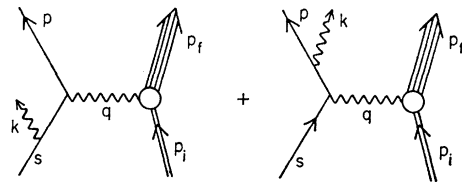


FIG. 10. Feynman diagrams for radiative ep inelastic scattering.

(only the scattered electron is detected):

$$\begin{aligned} d\sigma/d\Omega dp = & (2\alpha^2 E_p^2 M/q^4) \cos^2 \frac{1}{2}\theta [F(q^2, M_f^2) \\ & + (2/M^2) \tan^2 \frac{1}{2}\theta G(q^2, M_f^2)], \end{aligned} \quad (\text{B.1})$$

where E_s and E_p are energies of the incident and scattered electrons, respectively, M and M_f are masses of the initial and final hadronic system, θ is the scattering angle, and

$$q^2 = -4E_s E_p \sin^2(\theta/2),$$

$$M_f^2 = M^2 + 2M(E_s - E_p) + q^2.$$

When the mass of the final hadronic system is discrete, $M_f^2 = M_j^2$, we shall normalize the two form factors such that

$$F(q^2, M_f^2) = F_j(q^2) \delta(M_f^2 - M_j^2), \quad (\text{B.2a})$$

$$G(q^2, M_f^2) = G_j(q^2) \delta(M_f^2 - M_j^2), \quad (\text{B.2b})$$

where j denotes the j th discrete level, and $j=0$ corresponds to the elastic scattering. Substituting Eq. (B.2) into Eq. (B.1) and integrating both sides with respect to dp , we obtain the cross section

$$\begin{aligned} \frac{d\sigma_j}{d\Omega} = & \frac{\alpha^2 E_p^2}{q^4} [1 + E_s M^{-1}(1 - \cos\theta)]^{-1} \\ & \times \cos^2 \frac{1}{2}\theta \left[F_j(q^2) + \frac{2}{M^2} \tan^2 \frac{1}{2}\theta G_j(q^2) \right]. \end{aligned} \quad (\text{B.3})$$

The form factors $F_j(q^2)$ and $G_j(q^2)$ for elastic ep scattering are given in Eqs. (III.2) and (III.3), and those for the narrow-width approximation to the 3-3 resonance are given in Eq. (III.11) in the text. An example of the form factors $F(q^2, M_f^2)$ and $G(q^2, M_f^2)$ for continuous M_f^2 is given by Eqs. (III.5) and (III.6) for the 3-3 resonance.

In the following sections we first give the formula to calculate the radiative tail from a discrete level and then give a formula for calculating the radiative corrections to continuum states.

1. Radiative Tail from a Discrete Final Hadronic State

The expression for the radiative tail due to the j th level is [see Eq. (11) of Ref. 13]

$$\begin{aligned} \frac{d^2\sigma_{jr}}{d\Omega dp} = & \frac{\alpha^3 E_p}{(2\pi)^2 M E_s} \int_{-1}^1 \frac{\omega d(\cos\theta_k)}{2q^4(u_0 - |\mathbf{u}| \cos\theta_k)} \\ & \times \int_0^{2\pi} B_{\mu\nu} T_{\mu\nu} d\phi_k, \end{aligned} \quad (\text{B.4})$$

where

$$\begin{aligned}
 B_{\mu\nu}T_{\mu\nu} = & M^2 F_j(q^2) \left\{ \frac{-m^2}{(pk)^2} [2E_s(E_p + \omega) + \frac{1}{2}q^2] - \frac{m^2}{(sk)^2} [2E_p(E_s - \omega) + \frac{1}{2}q^2] - 2 \right. \\
 & + \frac{2}{(sk)(pk)} \{ m^2(s\dot{p} - \omega^2) + (ps)[2E_s E_p - (ps) + \omega(E_s - E_p)] \} \\
 & + (pk)^{-1} [2(E_s E_p + E_s \omega + E_p^2) + \frac{1}{2}q^2 - (s\dot{p}) - m^2] - (sk)^{-1} [2(E_s E_p - E_p \omega + E_s^2) + \frac{1}{2}q^2 - (s\dot{p}) - m^2] \Big\} \\
 & + G_j(q^2) \left(m^2(2m^2 + q^2) \{ [1/(pk)^2] + [1/(sk)^2] \} + 4 + \frac{4(ps)(ps - 2m^2)}{(pk)(sk)} + (2ps + 2m^2 - q^2)[(pk)^{-1} - (sk)^{-1}] \right),
 \end{aligned}$$

and q^2 is the momentum transfer to proton target squared, which is equal to

$$2m^2 - 2E_s E_p + 2 |\mathbf{s}| |\mathbf{p}| \cos \theta + 2M^2 - 2\omega(E_s - E_p) + 2\omega |\mathbf{u}| \cos \theta_k,$$

and ω is the photon energy equal to $\frac{1}{2}(u^2 - M_j^2)/(u_0 - |\mathbf{u}| \cos \theta_k)$. We have chosen a coordinate system such that the z axis is along the \mathbf{u} direction and the electron momenta \mathbf{s} and \mathbf{p} in the $x-z$ plane. In this coordinate system the quantities q^2 and M_j^2 are independent of the photon azimuthal angle ϕ_k , only (pk) and (sk) are dependent upon ϕ_k . Hence the integration over ϕ_k in Eq. (B.4) can be readily carried out with the help of the following three integration formulas:

$$\begin{aligned}
 (a) \quad & \int_0^{2\pi} \frac{d\phi_k}{a + bx} = \frac{2\pi}{(a^2 - b^2)^{1/2}} \quad \text{where } x = \cos \phi_k, \\
 (b) \quad & \int_0^{2\pi} \frac{d\phi_k}{(a + bx)^2} = \frac{2\pi a}{(a^2 - b^2)^{3/2}}, \\
 (c) \quad & \int_0^{2\pi} \frac{d\phi_k}{(a + bx)(a' + b'x)} = \frac{2\pi}{(a'b - ab')} \left[\frac{b}{(a^2 - b^2)^{1/2}} - \frac{b'}{(a'^2 - b'^2)^{1/2}} \right].
 \end{aligned}$$

The integrated result is given as the following:

$$\begin{aligned}
 \frac{d^2\sigma_{jr}}{d\Omega d\dot{p}} = & \frac{\alpha^3}{(2\pi)^2} \left(\frac{E_p}{E_s} \right) M^{-1} \int_{-1}^1 \frac{\omega d(\cos \theta_k)}{2q^4(u_0 - |\mathbf{u}| \cos \theta_k)} \\
 & \times \left(M^2 F_j(q^2) \left\{ \frac{-2\pi am^2}{(a^2 - b^2)^{3/2}} \left[2E_s(E_p + \omega) + \frac{q^2}{2} \right] - \frac{2\pi a'm^2}{(a'^2 - b'^2)^{3/2}} \left[2E_p(E_s - \omega) + \frac{q^2}{2} \right] - 4\pi \right. \right. \\
 & + 4\pi \left(\frac{\nu}{(a^2 - b^2)^{1/2}} - \frac{\nu'}{(a'^2 - b'^2)^{1/2}} \right) \{ m^2(s\dot{p} - \omega^2) + (s\dot{p})[2E_s E_p - (s\dot{p}) + \omega(E_s - E_p)] \} \\
 & + \frac{2\pi}{(a^2 - b^2)^{1/2}} \left[2(E_s E_p + E_s \omega + E_p^2) + \frac{q^2}{2} - (s\dot{p}) - m^2 \right] \\
 & \left. \left. - \frac{2\pi}{(a'^2 - b'^2)^{1/2}} \left[2(E_s E_p - E_p \omega + E_s^2) + \frac{q^2}{2} - (s\dot{p}) - m^2 \right] \right\} \right. \\
 & + G_j(q^2) \left[\left(\frac{2\pi a}{(a^2 - b^2)^{3/2}} + \frac{2\pi a'}{(a'^2 - b'^2)^{3/2}} \right) m^2(2m^2 + q^2) + 8\pi \right. \\
 & \left. + 8\pi \left(\frac{\nu}{(a^2 - b^2)^{1/2}} - \frac{\nu'}{(a'^2 - b'^2)^{1/2}} \right) (s\dot{p})(s\dot{p} - 2m^2) + 2\pi[(a^2 - b^2)^{-1/2} - (a'^2 - b'^2)^{-1/2}](2s\dot{p} + 2m^2 - q^2) \right], \quad (\text{B.5})
 \end{aligned}$$

where

$$\begin{aligned} \nu &= \frac{-|\mathbf{p}| \sin \theta_p}{\omega [E_p |\mathbf{s}| \sin \theta_s - E_s |\mathbf{p}| \sin \theta_p + |\mathbf{s}| |\mathbf{p}| \sin \theta \cos \theta_k]}, \\ \nu' &= \frac{-|\mathbf{s}| \sin \theta_s}{\omega [E_p |\mathbf{s}| \sin \theta_s - E_s |\mathbf{p}| \sin \theta_p + |\mathbf{s}| |\mathbf{p}| \sin \theta \cos \theta_k]}, \\ a &= \omega (E_p - |\mathbf{p}| \cos \theta_p \cos \theta_k), \\ b &= -\omega |\mathbf{p}| \sin \theta_p \sin \theta_k, \\ a' &= \omega (E_s - |\mathbf{s}| \cos \theta_s \cos \theta_k), \\ b' &= -\omega |\mathbf{s}| \sin \theta_s \sin \theta_k, \\ \theta_k &= \text{angle between } \mathbf{k} \text{ and } \mathbf{u}, \\ \theta_p &= \text{angle between } \mathbf{p} \text{ and } \mathbf{u}, \\ \theta_s &= \text{angle between } \mathbf{s} \text{ and } \mathbf{u}. \end{aligned}$$

and

$$\theta_s = \text{angle between } \mathbf{s} \text{ and } \mathbf{u}.$$

2. The Radiative Corrections to the Continuum State

Let us assume that the radiative tail due to the elastic peak has been subtracted from the inelastic spectrum already. The exact formula to lowest order in α (ignoring the radiative corrections to the hadron current) is given by Eq. (15) of Ref. 13. The radiative cross section (ignoring the straggling) can be written as

$$(d\sigma_r/d\Omega dp)(E_s, E_p) = (d\sigma/d\Omega dp)(E_s, E_p)[1 + \delta_r(\Delta)] + (d\sigma_r/d\Omega dp)(w > \Delta), \quad (\text{B.6})$$

where $d\sigma/d\Omega dp(E_s, E_p)$ is the continuum nonradiative cross section,

$$\delta_r(\Delta) = \frac{-\alpha}{\pi} \left[\frac{28}{9} - \frac{13}{6} \ln \frac{2(s\bar{p})}{m^2} + \left(\ln \frac{E_s}{\Delta} + \ln \frac{E_p}{\Delta} \right) \left(\ln \frac{2(s\bar{p})}{m^2} - 1 \right) - \Phi\left(-\frac{E_s - E_p}{E_p}\right) - \Phi\left(\frac{E_s - E_p}{E_s}\right) \right], \quad (\text{B.7})$$

$\Phi(x)$ is the Spence function, and

$$\frac{d\sigma_r}{d\Omega dp} (w > \Delta) = \frac{\alpha^3}{2\pi M E_s} \int_{-1}^1 d(\cos \theta_k) \int_{\Delta}^{\omega_{\max}(\cos \theta_k)} \frac{\omega d\omega}{q^4} \int_0^{2\pi} B_{\mu\nu}^c T_{\mu\nu} d\phi_k. \quad (\text{B.8})$$

$B_{\mu\nu}^c T_{\mu\nu}$ is the same as $B_{\mu\nu} T_{\nu\mu}$ in Eq. (B.4) except that $F_j(q^2)$ and $G_j(q^2)$ are replaced by $F(q^2, M_f^2)$ and $G(q^2, M_f^2)$, respectively. The energy ω of the photon is a function of M_f^2 and $\cos \theta_k$,

$$\omega = \frac{1}{2}(u^2 - M_f^2)/(u_0 - |\mathbf{u}| \cos \theta_k); \quad (\text{B.9})$$

$\omega_{\max}(\cos \theta_k)$ is the value for ω at the pion threshold

$$\omega_{\max}(\cos \theta_k) = \frac{1}{2}[u^2 - (M + m_\pi)^2]/(u_0 - |\mathbf{u}| \cos \theta_k). \quad (\text{B.10})$$

Let us sketch briefly the derivation of Eqs. (B.6)–(B.8). The continuum mass state can be regarded as a summation of many discrete levels. Hence, in order to obtain the radiative tail due to continuous mass states, we have to integrate Eq. (B.4) with respect to M_f^2 . Equivalently all we need to do is to make the replacement

$$F_j(q^2) \rightarrow \int_{(M+m_\pi)^2}^{u^2} F(q^2, M_f^2) dM_f^2 = \int_0^{\omega_{\max}(\cos \theta_k)} F(q^2, M_f^2) 2(u_0 - |\mathbf{u}| \cos \theta_k) d\omega \quad (\text{B.11})$$

and a similar one for $G_j(q^2)$ in Eq. (B.4). We have used Eq. (B.9) to change the variable of integration. Substituting Eq. (B.11) into Eq. (B.4), we notice that the integrand diverges at $\omega=0$ (the well-known infrared divergence). Hence we divide the integration into two parts, one from $\omega=0$ to Δ and the other from Δ to $\omega_{\max}(\cos \theta_k)$. The integration from Δ to $\omega_{\max}(\cos \theta_k)$ is given by Eq. (B.8). The integration from $\omega=0$ to Δ plus the vacuum polarization and the vertex correction is given by Eq. (B.7), which can be obtained from the

Z^0 terms of Eq. (II.6). It should be noted that Δ is chosen here to be independent of angle, whereas in Eq. (II.6) ΔE is the maximum energy loss of the detected electron. When ΔE is fixed, the maximum energy of photons which can be emitted along the direction of the incident electron is $\eta^2 \Delta E$, whereas in the direction of the scattered electron it is ΔE . Hence, instead of $[\ln(E_s/\eta^2 \Delta E) + \ln(E_p/\Delta E)]$ as in Eq. (II.6), we have to use $[\ln(E_s/\Delta) + \ln(E_p/\Delta)]$ in Eq. (B.7).

The integration with respect to ϕ_k in Eq. (B.8) is of

course identical to that in Eq. (B.5). Equation (B.8) is practically useless as it stands, because we have to know $F(q^2, M_f^2)$ and $G(q^2, M_f^2)$ for certain range of q^2 and M_f^2 before we can apply radiative corrections. We shall derive an approximate expression for Eq. (B.8) using peaking approximations in Appendix C. A possible use of Eq. (B.8) is in making the final consistency check on the data after $F(q^2, M_f^2)$ and $G(q^2, M_f^2)$ were extracted, by using peaking approximation method.

APPENDIX C: PEAKING APPROXIMATIONS

Schiff³¹ was the first one to use the so-called peaking approximation to integrate the Bethe-Heitler³² formula for bremsstrahlung. Our Eqs. (B.4) and (B.6) are essentially the Bethe-Heitler formula with modifications due to the spin, recoil and excitation of the target system.³³ Many people^{3,6-11} have written down various versions of the peaking approximations. In the following we shall derive our own version based on Eqs. (B.4) and (B.8). Figure 11(a)-11(c) show some examples of the integrands of Eqs. (B.5) for the radiative tail from the elastic peak in $e\mu$ scattering, for $E_s=20$ GeV, $\theta=5^\circ$, and $E_p=18, 12$, and 6 GeV. The interesting features shown in these plots are:

(1) The integrand in Eq. (B.5) is indeed very sharply peaked when θ_k is equal to θ_s or θ_p , namely most of the photons are emitted along the direction of either the incident or the scattered electron. The widths of the peaks are roughly given by $(m/E_s)^{1/2}$ and $(m/E_p)^{1/2}$, respectively. This is to be compared with $\bar{\theta}=m/E_s$, which is the angular spread of the bremsstrahlung when the direction of the scattered electron is integrated out. We shall call these two peaks the s peak and the p peak, respectively.

(2) Because $|q^2|$ decreases monotonically with increasing $\cos \theta_k$ and the integrand is roughly proportional to $q^{-4}G_p^2(q^2)$, we see that the s peak is more prominent than the p peak.

(3) When E_p is small, there occurs a third peak near $\cos \theta_k=1$, where $|q^2|$ becomes minimum. Since this third peak is not taken into account in the usual peaking approximation, we can understand why the peaking approximation becomes unreliable at the low-energy end of the scattered electron spectrum.

In Fig. 11(d)-11(f), some examples of the integrand in Eq. (B.5) are shown for the radiative tail from the elastic peak in $\mu\mu$ scattering with $E_s=20$ GeV, $\theta=5^\circ$, $E_p=18.3, 12.5$, and 6 GeV. We observe that there are hardly any peaks in this case. However, it is interesting to notice that if we blindly apply our peaking approximation formula, Eq. (C.11), to the calculation of the elastic radiative tail of $\mu\mu$ scattering, the answer is correct to within 10% near the elastic peak, and within a factor of 2 in the deep inelastic region.

The detailed procedure of our peaking approxima-

tion is as follows:

(1) Terms with $(sk)^{-2}$ and $(sk)^{-1}$ in Eq. (B.4) are assumed to contribute only to the s peak, whereas terms with $(pk)^{-2}$ and $(pk)^{-1}$ are assumed to contribute only to the p peak.

(2) Terms which do not have (pk) or (sk) in the denominator, such as -2 and 4 in Eq. (B.4), are made to contribute half to the s peak and half to the p peak.

(3) The most important terms are those with $(pk)(sk)$ in the denominator. We first ignore the θ_k dependence of photon energy, ω , and integrate this term with respect to the solid angle

$$\begin{aligned} \int \frac{d\Omega_k}{(pk)(sk)} &= \int_0^1 dx \int \frac{d\Omega_k}{(kp_x)^2} \\ &= \frac{4\pi}{\omega^2} [(sp)^2 - m^4]^{-1/2} \ln \frac{sp + [(sp)^2 - m^4]^{1/2}}{m^2} \\ &\simeq (4\pi/\omega^2) (sp)^{-1} \ln [2(sp)/m^2], \end{aligned}$$

where $p_x = (1-x)p + xs$.

We then give

$$\frac{2\pi}{\omega_s^2} (sp)^{-1} \ln \frac{2(sp)}{m^2}$$

to the s peak and

$$\frac{2\pi}{\omega_p^2} (sp)^{-1} \ln \frac{2(sp)}{m^2}$$

to the p peak, where ω_s and ω_p are the photon energies along the incident ($\theta_k=\theta_s$) and outgoing ($\theta_k=\theta_p$) electron directions, respectively, and are given explicitly by

$$\omega_s = \frac{1}{2}(u^2 - M_f^2)/[M - E_p(1 - \cos \theta)] \quad (C.1)$$

and

$$\omega_p = \frac{1}{2}(u^2 - M_f^2)/[M + E_s(1 - \cos \theta)]. \quad (C.2)$$

(4) Using a technique similar to the above, we obtain

$$\begin{aligned} \int \frac{m^2}{(pk)^2} d\Omega_k &= \frac{4\pi}{\omega_p^2}, \\ \int \frac{m^2}{(sk)^2} d\Omega_k &= \frac{4\pi}{\omega_s^2}, \\ \int \frac{d\Omega_k}{(pk)} &= \frac{4\pi}{\omega_p} p^{-1} \ln \frac{E_p + p}{m} \simeq \frac{4\pi}{\omega_p E_p} \ln \frac{2E_p}{m}, \\ \int \frac{d\Omega_k}{(sk)} &\simeq \frac{4\pi}{\omega_s E_s} \ln \frac{2E_s}{m}. \end{aligned}$$

The coefficients associated with these terms in the integrand are evaluated at the peaks. For example, for

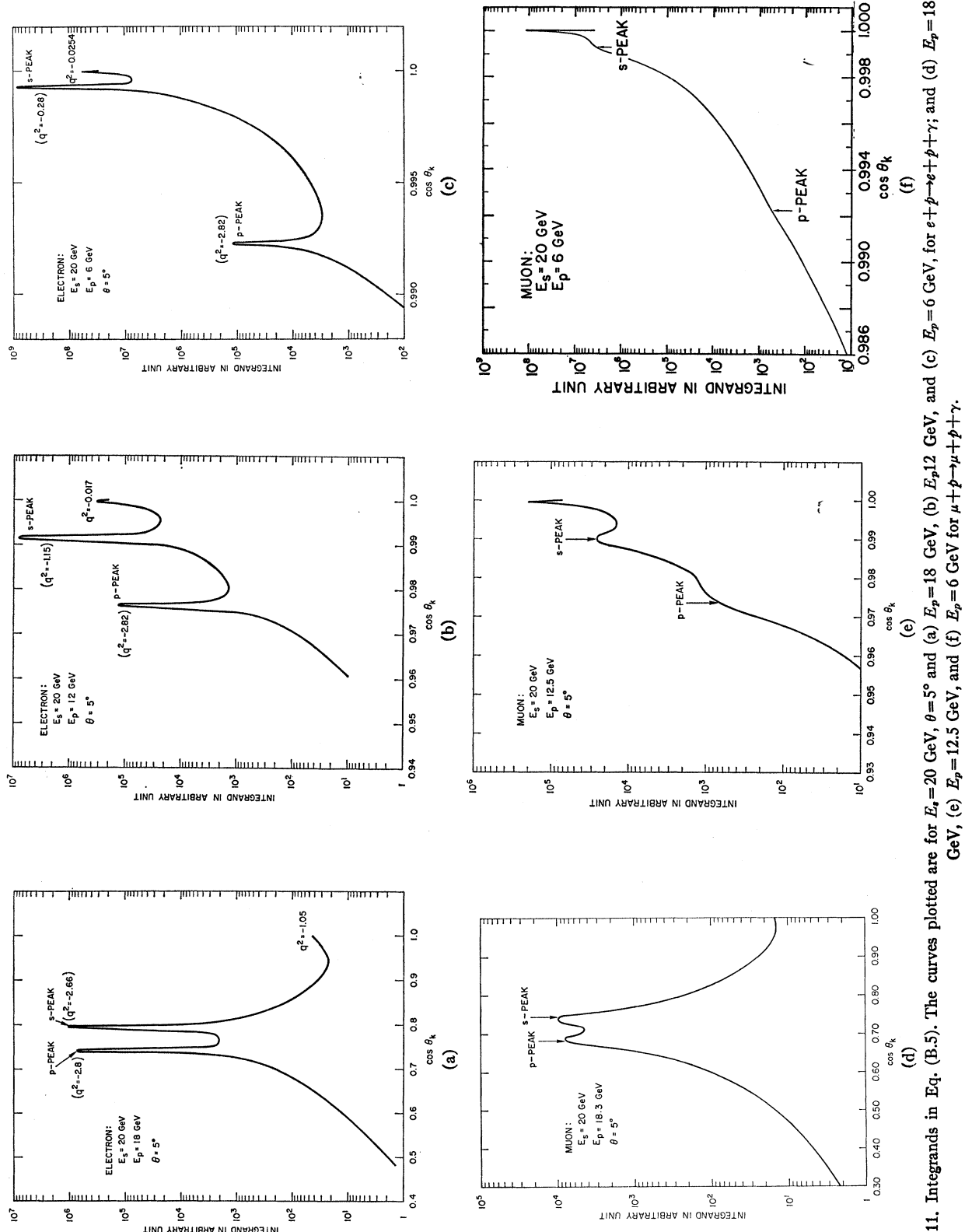


Fig. 11. Integrands in Eq. (B.5). The curves plotted are for $E_s = 20$ GeV, $\theta = 5^\circ$ and (a) $E_p = 18$ GeV, (b) $E_p = 12$ GeV, and (c) $E_p = 6$ GeV, for $e + p \rightarrow e + p + \gamma$; and (d) $E_p = 18.3$ GeV, (e) $E_p = 12.5$ GeV, and (f) $E_p = 6$ GeV for $\mu + p \rightarrow \mu + p + \gamma$.

the s peak, ω is replaced by ω_s , q^2 and M_f^2 are replaced by

$$\begin{aligned} q_s^2 &= -2(E_s - \omega_s)E_p(1 - \cos\theta), \\ M_{fs}^2 &= u^2 - 2\omega_s(u_0 - |\mathbf{u}| \cos\theta_s), \end{aligned} \quad (\text{C.3})$$

and for the p peak, ω is replaced by ω_p , and q^2 and M_f^2

are replaced by

$$\begin{aligned} q_p^2 &= -2E_s(E_p + \omega_p)(1 - \cos\theta), \\ M_{fp}^2 &= u^2 - 2\omega_p(u_0 - |\mathbf{u}| \cos\theta_p). \end{aligned} \quad (\text{C.4})$$

With these approximations, Eq. (B.8) can be written as

$$\frac{d\sigma_r}{d\Omega dp} (\omega > \Delta) = \left(\frac{d\sigma_r}{d\Omega dp} (\omega > \Delta) \right)_{k||s} + \left(\frac{d\sigma_r}{d\Omega dp} (\omega > \Delta) \right)_{k||p}, \quad (\text{C.5})$$

where

$$\begin{aligned} \left(\frac{d\sigma_r}{d\Omega dp} (\omega > \Delta) \right)_{k||s} &= \frac{\alpha^3 E_p M}{2\pi E_s} \int_{\Delta}^{\omega_{\max}(\cos\theta_s)} \frac{d\omega_s}{\omega_s} \frac{1}{q_s^4} (F(q_s^2, M_{fs}^2) \{-E_p(E_s - \omega_s)(1 + \cos\theta) - \omega_s^2 \\ &\quad + [E_p(E_s - \omega_s)(1 + \cos\theta) + \omega_s(E_s + E_p \cos\theta)] \ln[2(sp)/m^2] \\ &\quad + [-\omega_s(E_s + E_p \cos\theta) + (E_p/E_s)\frac{1}{2}(\omega_s^2)(1 + \cos\theta)] \ln(4E_s^2/m^2)\} \\ &\quad + [2G(q_s^2, M_{fs}^2)/M^2] \{-E_p(E_s - \omega_s)(1 - \cos\theta) + \omega_s^2 + E_s E_p(1 - \cos\theta) \ln[2(sp)/m^2] \\ &\quad - (\omega_s/E_s)E_p(1 - \cos\theta)(E_s - \frac{1}{2}\omega_s) \ln(2E_s/m)^2\}); \end{aligned} \quad (\text{C.6a})$$

$$\left(\frac{d\sigma_r}{d\Omega dp} (\omega > \Delta) \right)_{k||p} = \frac{\alpha^3 E_p M}{2\pi E_s} \int_{\Delta}^{\omega_{\max}(\cos\theta_p)} \frac{d\omega_p}{\omega_p} \frac{1}{q_p^4} \times [\text{terms obtained by interchanges } E_s \leftrightarrow E_p,$$

$$\omega_s \leftrightarrow -\omega_p, \text{ and } q_s^2 \leftrightarrow q_p^2 \text{ in Eq. (C.6a)}]. \quad (\text{C.6b})$$

(5) We have gotten rid of one integration by the above approximation; however, Eq. (C.6) is still not in a desirable form because it still implies that $F(q^2, M_f^2)$ and $G(q^2, M_f^2)$ have to be separated out from the cross section for certain ranges of q^2 and M_f^2 before one can apply radiative corrections. It is desirable to make a further approximation such that the integrands in Eqs. (C.6a) and (C.6b) contain only the cross sections $\sigma(E_s - \omega_s, E_p)$ and $\sigma(E_s, E_p + \omega_p)$, respectively. Comparison of Eq. (C.6) with Eq. (B.1) shows that somehow we have to make the ratio of the coefficient of $G_j(q^2)$ to that of $F_j(q^2)$ in Eq. (C.6) equal to $2M^{-2} \tan^2(\theta/2)$ in order to achieve this purpose. We can do this by ignoring ω_s^2 in the nonlogarithmic term and changing $\ln(4E_s^2/m^2)$ into $\ln[2(sp)/m^2]$ in Eq. (C.6a). After these approximations, Eq. (C.5) can be written as

$$\begin{aligned} \frac{d\sigma_r}{d\Omega dp} (\omega > \Delta) &= \int_{E_{s \min}(E_p)}^{E_s - \Delta} \frac{dE'_s}{E_s - E'_s} t_s \frac{d\sigma}{d\Omega dp} (E'_s, E_p) \\ &\quad + \int_{E_p + \Delta}^{E_{p \max}(E_s)} \frac{dE'_p}{E'_p - E_p} t_p \frac{d\sigma}{d\Omega dp'} (E_s, E'_p), \end{aligned} \quad (\text{C.7})$$

where

$$t_{s,p} = \frac{\alpha}{\pi} \left\{ \frac{1}{2} (1 + x_{s,p}^2) \ln[2(sp)/m^2] - x_{s,p} \right\}, \quad (\text{C.8})$$

$$x_s = E'_s/E_s = (E_s - \omega_s)/E_s, \quad (\text{C.9a})$$

$$x_p = E_p/E'_p = E_p/(E_p + \omega_p), \quad (\text{C.9b})$$

and $E_{s \min}(E_p)$ and $E_{p \max}(E_s)$ are given by Eqs. (A.18) and (A.19).

When M_f is discrete, $M_f = M_j$, $d\sigma/d\Omega dp$ in Eq. (C.7) contains a δ function

$$\begin{aligned} (d\sigma/d\Omega dp') (E'_s, E'_p) &\rightarrow [d\sigma_j(E'_s)/d\Omega] \\ &\times [2M + 2E'_s(1 - \cos\theta)] \delta[(s' + p_i - p')^2 - M_j^2]. \end{aligned} \quad (\text{C.10})$$

Substituting Eq. (C.10) into Eq. (C.7), we obtain the expression for the radiative tail from a discrete hadronic mass state $M_f = M_j$ in the peaking approximation:

$$\begin{aligned} \frac{d\sigma_{jr}}{d\Omega dp} (E_s, E_p) &= \omega_s^{-1} t_s \frac{M + (E_s - \omega_s)(1 - \cos\theta)}{M - E_p(1 - \cos\theta)} \\ &\times \frac{d\sigma_j}{d\Omega} (E_s - \omega_s) + \omega_p^{-1} t_p \frac{d\sigma_j}{d\Omega} (E_p), \end{aligned} \quad (\text{C.11})$$

where ω_s and ω_p are given by Eqs. (C.1) and (C.2), respectively.

APPENDIX D: REMARKS ON PROGRAMMING

In this Appendix, a few remarks concerning the numerical calculations of radiative corrections will be given.

First, it should be noted that in calculating the radiative tail from the elastic peak, the integrand in Eq. (B.5) has an uncertainty of zero divided by zero when $a'b = ab'$. This happens just because of the particular factorization used in the ϕ_k integration, and there is nothing wrong with it. It occurs at an angle given by

$$\cos\theta_k = (1/\sin\theta)[(E_s/|\mathbf{s}|) \cos\theta_p - (E_p/|\mathbf{p}|) \sin\theta_s],$$

which corresponds to the position of the minimum between the s and the p peaks. To facilitate the numerical calculation, an extremely small area near this point should be ignored in the numerical integration. The error thus introduced is negligible.

Secondly, in calculating the radiative corrections in the inelastic region, two small regions near point a and b as shown in Fig. 3 should be ignored in the integration. This will avoid difficulty caused by roundoff error in a computer. Again, the error thus introduced is beyond detection, because typically the deleted region is only a few MeV wide.

We have performed all the calculations discussed in this paper on the IBM 360/75 computer at SLAC. Double precision has been used all through the calculations in order to retain 14 significant digits. Typically, we found the following information which may be of some use to the experimentalists:

- (1) It takes 0.74 min to compute 200 different values of the Spence function with an accuracy of 10^{-6} .
- (2) It takes ≈ 0.6 min to compute 10 different values of δ for $e\bar{p}$ elastic scattering using Tsai's formula, while ≈ 0.5 min for the same number of points using the formula given by Meister and Yennie.
- (3) It takes 1.5 min to calculate 100 points for the radiative corrections on the 3-3 resonance peak with an accuracy of better than 10^{-4} , using the peaking approximation method.
- (4) It takes 4.2 min to calculate 175 points on the radiative tail from the $e\bar{p}$ elastic peak with an accuracy of better than 10^{-3} , using the exact formula.
- (5) It takes ~ 45 min to completely unfold ~ 1100 data points of the four spectra shown in Fig. 5(a)-5(d). The time needed to compute the elastic radiative tails is not included.
- (6) It takes only ~ 2 min to unfold one spectrum shown in Fig. 5(e) or 5(f) by the approximation that the two integrals in Eq. (VI.2) are equal to each other.

REFERENCES

- ¹ J. D. Bjorken, Phys. Rev. **163**, 1767 (1967).
- ² Y. Nambu and E. Shrauner, Phys. Rev. **128**, 862 (1962); S. L. Adler and F. J. Gilman, *ibid.* **152**, 1460 (1966).
- ³ A. A. Cone, K. W. Chen, J. R. Dunning, Jr., G. Hartwig, N. F. Ramsey, J. K. Walker, and R. Wilson, Phys. Rev. **156**, 1490 (1967).
- ⁴ F. W. Brasse, J. Engler, E. Ganssauge, and M. Schweizer, Abstract 238, presented at Heidelberg International Conference on Elementary Particles, 20-27 September 1967; W. K. H. Panofsky, Rapporteur's talk in the same conference.
- ⁵ L. I. Schiff, Phys. Rev. **87**, 750 (1952).
- ⁶ L. N. Hand, Phys. Rev. **129**, 1834 (1963).
- ⁷ E. A. Allton, Phys. Rev. **135**, B570 (1964).
- ⁸ J. D. Bjorken, Ann. Phys. (N.Y.) **24**, 201 (1963).
- ⁹ J. P. Perez-y-Jorba, J. Phys. Radium **22**, 733 (1961).
- ¹⁰ H. Nguyen-Ngoc and J. P. Perez-y-Jorba, Phys. Rev. **136**, B1036 (1964).
- ¹¹ N. T. Meister and T. A. Griffy, Phys. Rev. **133**, B1032 (1964).
- ¹² L. C. Maximon and D. B. Isabelle, Phys. Rev. **133**, B1344 (1964).
- ¹³ Y. S. Tsai, *Proceedings of Nucleon Structure Conference at Stanford (1963)*, R. Hofstadter and L. I. Schiff, Eds. (Stanford University Press, Stanford, Calif., 1964), p. 221.
- ¹⁴ Y. S. Tsai, Phys. Rev. **122**, 1898 (1961).
- ¹⁵ N. T. Meister and D. R. Yennie, Phys. Rev. **130**, 1210 (1963).
- ¹⁶ A. J. Dufner and Y. S. Tsai, Phys. Rev. **168**, 1801 (1968).
- ¹⁷ J. Schwinger, Phys. Rev. **76**, 760 (1949). The analytical form for $f(\theta)$ in terms of Spence function $\Phi(x)$ was given by G. Källén, in *Hnadbuch der Physik*, S. Flügge, Ed. (Springer-Verlag, Berlin, 1958), Vol. 5, Pt. 1, p. 169.
- ¹⁸ D. R. Yennie and H. Suura, Phys. Rev. **105**, 1378 (1957).
- ¹⁹ D. R. Yennie, S. Frautschi, and H. Suura, Ann. Phys. (N.Y.) **13**, 379 (1961).
- ²⁰ K. Mitchell, Phil. Mag. **40**, 351 (1949).
- ²¹ See Footnote 21 of Ref. 14.
- ²² Y. S. Tsai, Phys. Rev. **120**, 269 (1960). See expression $f(x)$ following Eq. (17) of this reference.
- ²³ K. E. Erickson, Nuovo Cimento **19**, 1029 (1961). See also Errata in K. E. Erickson, Nuovo Cimento **21**, 383 (1961).
- ²⁴ T. Janssens, R. Hofstadter, E. B. Hughes, and M. R. Yearian, Phys. Rev. **142**, 922 (1966); M. Goitein, R. J. Budnitz, L. Carroll, J. Chen, J. R. Dunning, Jr., K. Hanson, D. Imrie, C. Mistretta, J. K. Walker, Richard Wilson, G. F. Dell, M. Fotino, J. M. Peterson, and H. Winick, Phys. Rev. Letters **18**, 1016 (1967); W. Bartel, B. Dudelzak, H. Krehbiel, J. M. McElroy, U. Meyer-Berkout, R. J. Morrison, H. Nguyen-Ngoc, W. Schmidt, and G. Weber, *ibid.* **17**, 608 (1966); W. Albrecht, H.-J. Behrend, H. Dorner, W. Flauger, and H. Hultschig, *ibid.* **18**, 1014 (1967); D. H. Coward, H. DeStaeler, R. A. Early, J. Litt, A. Minten, L. W. Mo, W. K. H. Panofsky, R. E. Taylor, M. Breidenbach, J. I. Friedman, H. W. Kendall, P. N. Kirk, B. C. Barish, J. Mar, and J. Pine, *ibid.* **20**, 292 (1968).
- ²⁵ L. Hand (Ref. 6). There are obvious misprints in Eq. (7) and (8) of this reference. We believe our Eq. (III.12) is what is meant by the author. It should be noted also that our version of peaking approximation formula was derived from Eqs. (B.4) and (B.8) which are valid for arbitrary final hadronic states, whereas the formula given in Refs. 6 and 7 are valid only for calculating the radiative tail from the elastic peak.
- ²⁶ E. D. Bloom, D. H. Coward, H. DeStaeler, J. Dress, J. Litt, G. Miller, L. W. Mo, R. E. Taylor, M. Breidenbach, J. I. Friedman, G. C. Hartmann, H. K. Kendall, and S. C. Loken, *Proceedings of the International Conference on High Energy Physics*, Vienna, 1968, J. Prentki and J. Steinberger, Eds. (CERN, Scientific Information Service, Geneva, 1968), Contributed Paper No. 563; W. K. H. Panofsky, *ibid.*, p. 23.
- ²⁷ H. A. Bethe and W. Heitler, Proc. Roy. Soc. (London), **A146**, 83 (1934). See also W. Heitler, *The Quantum Theory of Radiation* (Oxford University Press, London, 1954); 3rd ed., Eq. 15, p. 378.
- ²⁸ L. Eges, Phys. Rev. **76**, 264 (1949). The analytical method of obtaining the Bethe and Heitler straggling formula was first used in this reference.
- ²⁹ Y. S. Tsai and V. Whitis, Phys. Rev. **149**, 1248 (1966). We use the notations of this reference.
- ³⁰ H. A. Bethe and J. Ashkin, in *Experimental Nuclear Physics*, E. Segre, Ed. (John Wiley & Sons, Inc., New York, 1953), p. 265.
- ³¹ L. I. Schiff, Phys. Rev. **87**, 750 (1952).
- ³² W. Heitler, *The Quantum Theory of Radiation* (Oxford University Press, London, 1954); 3rd ed., p. 244.
- ³³ Various modified versions of Bethe-Heitler formula have been given by various authors. R. A. Berg and C. N. Lindner [Phys. Rev. **112**, 2072 (1958)] gave a formula for treating the radiative tail from the elastic peak of proton. Unfortunately, their final results seem to depend upon the assumption that the Dirac form factor $F_1(q^2)$ and the Pauli form factor $F_2(q^2)$ for the proton are equal to each other. Since this is no longer true at high $|q^2|$, their formula cannot be used for high-energy experiments. E. S. Ginsberg and R. H. Pratt [Phys. Rev. **134**, B773 (1964); **137**, B1500 (1965)] gave a formula for calculating the elastic radiative tail from a nucleus with arbitrary charge and magnetic form factors, neglecting the recoil. The formulas in Ref. 13 and our Appendix B supersede all these formulas because our formulas are correct for an arbitrary target spin, arbitrary final hadronic states (elastic or inelastic), and arbitrary form factors, all with correct relativistic kinematics.
- ³⁴ L. C. Maximon and C. Tzara, Phys. Letters **26B**, 201 (1968).